arXiv:1505.06568v2 [hep-ph] 15 Aug 2015

MITP/15-034

Lepton-mass effects in the decays $H \to ZZ^* \to \ell^+\ell^-\tau^+\tau^-$ and $H \to WW^* \to \ell\nu\tau\nu_\tau$

S. Berge[1], S. Groote[2,3], J.G. Körner[3] and L. Kaldamäe[2]

[1] Institut für Theoretische Physik, RWTH Aachen University, 52056 Aachen, Germany

[2] Loodus- ja Tehnoloogiateaduskond, Füüsika Instituut,

Tartu Ülikool, Tähe 4, 51010 Tartu, Estonia

[3] PRISMA Cluster of Excellence, Institut für Physik,

Johannes-Gutenberg-Universität, Staudinger Weg 7, 55099 Mainz, Germany

Abstract

We consider τ-lepton mass effects in the cascade decays $H \to Z(\to \ell^+\ell^-) + Z^*(\to \tau^+\tau^-)$ and $H \to W^-(\to \ell^-\bar{\nu}_\ell) + W^{+*}(\to \tau^+\nu_\tau)$. Since the scale of the problem is set by the off-shellness q^2 of the respective gauge bosons in the limits $(m_\ell + m_{\ell'})^2 \leq q^2 \leq (m_H - m_{W,Z})^2$ and not by $m^2_{W,Z}$, lepton-mass effects are non-negligible for the τ modes in particular close to the threshold of the off-shell decays. Lepton-mass effects show up in the rate and in the three-fold joint angular decay distribution for the decays. Nonzero lepton masses lead to leptonic helicity-flip contributions which in turn can generate novel angular dependencies in the respective three-fold angular decay distributions. Lepton-mass effects are more pronounced in the $H \to Z(\to \ell\ell)Z^*(\to \tau\tau)$ mode which, in part, is due to the fact that the ratio of lepton helicity-flip/nonflip contributions in the decay $Z^* \to \ell^+\ell^-$ is four times larger than in the decay $W^{+*} \to \ell^+\nu$. Overall the inclusion of τ mass effects leads to a 3.97% reduction in the leptonic $H \to ZZ^*$ rate. Lepton mass effects are quite pronounced for q^2 values

from threshold up to $\sim 200\,\mathrm{GeV}^2$. For example, at $q^2 = 50\,\mathrm{GeV}^2$ the transverse–longitudinal–scalar helicity composition of the off-shell Z–boson changes from $0.06 : 0.94 : 0$ to $0.04 : 0.65 : 0.31$ for the τ lepton. This has observational consequences for the angular decay distributions of the final-state leptons. We also briefly consider the corresponding off-shell – off-shell decays $H \to Z^*(\to \ell^+\ell^-) + Z^*(\to \tau^+\tau^-)$ and $H \to W^{-*}(\to \ell^-\bar{\nu}_\ell) + W^{+*}(\to \tau^+\nu_\tau)$.

1 Introduction

We consider lepton-mass effects in the off-shell decays of gauge bosons in the processes $Z^* \to \tau^+\tau^-$ and $W^{+*} \to \tau^+\nu_\tau$ where the off-shell gauge bosons W^{+*}, Z^* are produced in the Higgs decays $H \to ZZ^*$, W^-W^{+*}. In the $H \to ZZ^*$ case the corresponding $\ell = e, \mu$ modes have recently been observed at the LHC and are therefore adequately dubbed "Higgs discovery channels" [1, 2]. Further evidence on these decays has been presented in Ref. [3]. The quantum numbers of the Higgs boson have been pinned down by an angular analysis of the four leptons in the final state to be $J^P = 0^+$ both in the leptonic $H \to ZZ^*$ mode [3, 4, 5] as well as in the leptonic $H \to W^-W^{+*}$ mode [6]. On the theoretical side there have been a number of papers analyzing the quantum numbers of the Higgs boson through an angular analysis of the four-lepton final state among which are Refs. [7, 8, 9, 10, 11, 12, 13, 14, 15, 16, 17, 18, 19]. The physics of the Higgs boson in all its aspects has been nicely reviewed in three recent papers [20, 21, 22].

Off-shell effects in the decays involving massive leptons will lead to additional scalar and scalar–longitudinal interference contributions well familiar from neutron beta decay, the semileptonic decay $\Xi^0 \to \Sigma^+\mu^-\bar{\nu}_\mu$ [23], or from the decays $B \to D^{(*)}\tau\nu_\tau$ [24, 25] and $\Lambda_b \to \Lambda_c\tau\nu_\tau$ [26]. The scalar and scalar–longitudinal interference contributions are quadratic in the lepton masses and can thus be neglected at the scale $m^2_{W,Z}$. However, for the off-shell decays $H \to ZZ^*, W^-W^{+*}$ the scale is not set by $m^2_{W,Z}$ but by the off-shellness of the respective gauge bosons which extends from threshold $q^2 = (m_\ell + m_{\ell'})^2$ (maximal recoil point) to the zero recoil point at $q^2 = (m_H - m_{W,Z})^2$, i.e. one has

$$(m_\ell + m_{\ell'})^2 \leq q^2 \leq (m_H - m_{W,Z})^2 \,. \tag{1}$$

One will therefore have to carefully consider τ-lepton mass effects particularly in the q^2 region close to threshold given by $q^2 = 4m_\tau^2$ and $q^2 = m_\tau^2$ for the leptonic modes in the decays $H \to ZZ^*$ and $H \to WW^*$, respectively. Lepton-mass effects reduce the overall rate relative to the zero lepton-mass case. In addition, lepton-mass effects lead to

leptonic helicity-flip contributions which in turn can generate novel angular dependencies in the respective angular decay distributions. These angular dependencies can mimic new angular terms introduced by higher dimension effective coupling terms [14, 15, 16] or non-SM (HVV) coupling terms [17, 18, 19]. τ-lepton mass effects should therefore not be neglected if one is aiming for high precision physics in the Higgs sector.[1]

Our paper is structured as follows. After this introductory section, in Sec. 2 we present a general formula for the three-fold angular angular decay distribution for the on-shell – off-shell decays $H \to VV^* \to \ell\ell\ell\ell$. The angular decay distribution is obtained using helicity methods. In Sec. 3 we discuss lepton-mass effects in the decay $H \to ZZ^* \to \ell\ell\tau\tau$ and their effect on the rates and the angular decay distributions. We do the same in Sec. 4 for the decays $H \to W^-W^{+*} \to \ell\nu_\ell\tau\nu_\tau$. In Sec. 5 we summarize our results and conclude with some general remarks. Some technical material regarding helicity amplitudes is relegated to the Appendices. In Appendix A we list the helicity amplitudes for the $H \to VV^*$ transitions. The helicity representation of the lepton tensors in the neutral- and charged-current cases can be found in Appendix B and C, respectively.

2 General formalism

The three-fold angular decay distribution in the cascade decays $H \to VV^* \to \ell\ell\ell\ell, \quad V = Z, W$ can be derived from the covariant contraction of the on-shell and off-shell lepton tensors $L^{(p)}_{\mu\nu}$ and $L^{(q)}_{\mu\nu}$ with the (HVV) Higgs coupling $H_{\alpha\beta}$ where the vertices are connected by the propagator projectors $P_1^{\alpha\mu}$ (spin 1) and $P_{0\oplus1}^{\nu\beta}$ (spin $0 \oplus 1$). One has

$$W(\theta_p, \theta_q, \chi) = H_{\alpha\alpha'}\, P_1^{\alpha\mu}(p)\, P_{0\oplus1}^{\alpha'\mu'}(q)\, L^{(p)}_{\mu\nu}(p)\, L^{(q)}_{\mu'\nu'}(q)\, P_1^{\nu\beta}(p)\, P_{0\oplus1}^{\nu'\beta'}(q)\, H^*_{\beta\beta'} \tag{2}$$

where, in the Standard Model (SM), $H_{\alpha\alpha'} = g_{\alpha\alpha'}$. We denote the on-shell and off-shell momenta of the gauge bosons by p and q. In the unitary gauge the on-shell spin-1 propagator

[1] Lepton-mass effects in the rate $H \to W\ell\nu$ and $H \to Z\ell\ell$ are also taken into account in Ref. [27].

$P_1^{\alpha\mu}$ ($p^2 = m_V^2$) and the off-shell propagator $P_{0\oplus1}^{\nu\beta}$ ($q^2 \neq m_V^2$) read

$$P_1^{\alpha\mu}(p) = -g^{\alpha\mu} + \frac{p^\alpha p^\mu}{p^2}, \qquad P_{0\oplus1}^{\nu\beta}(q) = -g^{\nu\beta} + \frac{q^\nu q^\beta}{m_V^2}. \tag{3}$$

Note that in the unitary gauge[2] the off-shell propagator $P_{0\oplus1}^{\nu\beta}(q)$ contains a spin-1 and a spin-0 piece. This can be seen by splitting the off-shell gauge propagator in Eq. (3) into its spin-1 and spin-0 components according to

$$P_{0\oplus1}^{\nu\beta}(q) = -g^{\nu\beta} + \frac{q^\nu q^\beta}{m_V^2} = \underbrace{\left(-g^{\nu\beta} + \frac{q^\nu q^\beta}{q^2}\right)}_{\text{spin 1}} - \underbrace{\frac{q^\nu q^\beta}{q^2} F_S(q^2)}_{\text{spin 0}}, \tag{4}$$

where

$$F_S(q^2) = \left(1 - \frac{q^2}{m_V^2}\right). \tag{5}$$

In the zero lepton-mass approximation one has $q^\mu L_{\mu\nu} = 0$ and therefore the spin-0 piece in Eq. (4) does not contribute and can be dropped when evaluating Eq. (2). This is always a good approximation for $\ell = e, \mu$ but no longer a good approximation for $\ell = \tau$. An interesting observation concerns the spin-0 contribution. Taken together with the propagator pole proportional to $(q^2 - m_V^2)^{-1}$, the contribution of the spin-0 piece can be seen to be proportional to a contact interaction of the form $(HV\psi\bar{\psi})$ with a q^2-dependent coupling when one sets $\Gamma_Z = 0$.

Technically there are two routes to obtain angular decay distributions from Eq. (2). In the first route one parametrizes the four-vectors of the problem in terms of the five phase-space variables $p^2 = m_V^2$, q^2, $\cos\theta_p$, $\cos\theta_q$ and χ (cf. Figs. 1 and 7). The covariant evaluation of the Lorentz-invariant expression (2) leads to a number of scalar products of momenta that are defined in different reference frames. When doing the requisite contractions, the

[2]The choice of the unitary gauge is mandatory to obtain a gauge-independent result. This can be seen by considering a general covariant R_ξ gauge where one has to consider Goldstone boson exchange in addition to gauge boson exchange. In the coupling to the final state fermion pair the gauge parameter ξ cancels between the Goldstone and gauge boson contributions, resulting in the unitary gauge propagator. This has been explicitly demonstrated for fermion–fermion scattering [28] and for the decay $t \to b + W^{+*}$ [29].

four-momenta have to be boosted to a common reference frame as e.g. described in Ref. [14] for the decay $H \to Z\ell\ell$ and in Ref. [30, 31] for the decay $K^\pm \to \pi^\pm\pi^0 e^+ e^-$. One then arrives at the desired three-fold joint angular decay distribution.

A second, perhaps more intelligent route, is to use an analysis in terms of helicity amplitudes. The advantage of the helicity method is that the origin of the angular factors multiplying the helicity structure functions can be straightforwardly identified. The angular factors can be seen to arise from the transformation properties of the helicity amplitudes under the action of the rotation group.

In order to transform to the helicity representation of the covariant form in Eq. (2) one makes use of the completeness relation for the spin-1 on-shell and off-shell polarization vectors. The on-shell and off-shell propagator can be expanded according to [25, 32]

$$P_1^{\alpha\mu}(p) = -g^{\alpha\mu} + \frac{p^\alpha p^\mu}{p^2} = \sum_{\lambda_V=\pm1,0} \bar{\varepsilon}^\alpha(\lambda_V)\bar{\varepsilon}^{*\,\mu}(\lambda_V) \tag{6}$$

($p^2 = m_V^2$) and

$$P_{0\oplus1}^{\mu'\alpha'}(q) = -g^{\mu'\alpha'} + \frac{q^{\mu'}q^{\alpha'}}{m_V^2} = -\sum_{\lambda_{V^*}=t,\pm1,0} \varepsilon^{\mu'}(\lambda_{V^*})\varepsilon^{*\,\alpha'}(\lambda_{V^*})\,\hat{g}_{\lambda_{V^*}\lambda_{V^*}}. \tag{7}$$

Note that there is an additional spin-0 degree of freedom propagating in the off-shell propagator in Eq. (7). We shall specify this spin-0 degree of freedom by assigning the label $\lambda_V = t$ (t for time-component) to this mode. According to the separation in Eq. (4) the "t" mode carries the weight $F_S = (1 - q^2/m_V^2)$ which finally leads to $\hat{g}_{\lambda_{V^*}\lambda_{V^*}} = diag\,\{F_S, -1, -1, -1\}$ in Eq. (7). The four polarization four-vectors $\varepsilon^\mu(t, \pm1, 0)$ will be specified in Appendix A.

In low-energy calculations such as neutron β decay or in the semileptonic bottom-hadron decays one usually drops the term proportional to (q^2/m_V^2) in Eq. (5) since one has $q^2 \ll m_V^2$. However, in the present application the factor (q^2/m_V^2) can become as large as 30% at the zero recoil point and can therefore not be neglected.[3]

[3]In muon decays $\mu^- \to e^- + \mu_\mu + \bar{\nu}_e$ where one is aiming for ultrahigh precision, the importance of the q^2/m_W^2 contributions have been discussed in the literature [33, 34].

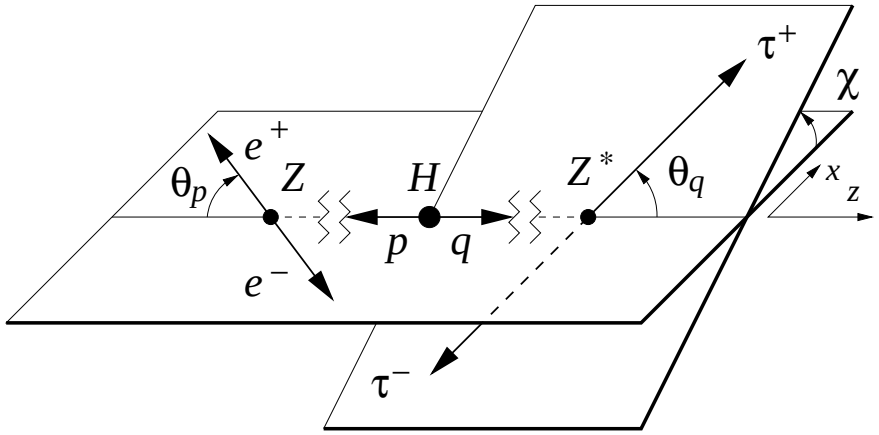


Figure 1: Definition of the momenta p and q, the polar angles θ_p and θ_q, and the azimuthal angle χ in the cascade decay $H \to Z(\to e^+e^-) + Z^*(\to \tau^+\tau^-)$

With the help of the completeness relations (6) and (7) the covariant form of the angular decay distribution (2) can be cast into a representation in terms of helicity components. One has

$$W(\theta_p, \theta_q, \chi) = \sum_{\substack{\lambda_V, \lambda'_V = \pm 1, 0 \\ \lambda_{V^*}, \lambda'_{V^*} = t, \pm 1, 0}} (-F_S)^{2-J-J'} L^{(p)}_{\lambda_V \lambda'_V}(\cos\theta_p) H_{\lambda_V, \lambda_{V^*}} H^*_{\lambda'_V, \lambda'_{V^*}} L^{(q)}_{\lambda_{V^*} \lambda'_{V^*}}(\cos\theta_q, \chi), \tag{8}$$

where $J = 1$ for $\lambda_V = \pm 1, 0$, $J = 0$ for $\lambda_V = t$ and correspondingly for the primed quantities. It turns out that $J = J'$ in the decay $H \to Z(\to e^+e^-) + Z^*(\to \tau^+\tau^-)$ as long as one is not analyzing τ-polarization effects, i.e. there are no spin-0 – spin-1 interference effects in this decay.

The evaluation of the helicity components of the $H \to VV^*$ transition amplitudes $H_{\lambda_V, \lambda_{V^*}}$ is given in Appendix A while the evaluation of the helicity components of the lepton tensors $L^{(p)}_{\lambda_V \lambda'_V}(\cos\theta_p)$ and $L^{(q)}_{\lambda_{V^*} \lambda'_{V^*}}(\cos\theta_q, \chi)$ are given in Appendix B (neutral-current case) and C (charged-current case).

Up to this point we have allowed for a general structure of the (HVV) coupling. In the following we shall specify to the SM coupling with $H_{\alpha\alpha'} = g_{\alpha\alpha'}$.

3 The four-body decay $H \to Z(\to \ell^+\ell^-) + Z^*(\to \tau^+\tau^-)$

In this section we write down the three-fold angular decay distribution of the decay $H \to Z(\to \ell^+\ell^-) + Z^*(\to \tau^+\tau^-)$ involving two different pairs of leptons, i.e. we assume $\ell \neq \tau$. The corresponding decay $H \to Z(\to \ell^+\ell^-) + Z^*(\to \ell^+\ell^-)$ involving two pairs of identical leptons (with and without lepton-mass effects) is more difficult to analyze due to the presence of nonfactorizing interference contributions. These identical-particle effects will be treated in a separate paper [35].

3.1 Three-fold angular decay distribution for the four-body decay $H \to Z(\to \ell^+\ell^-) + Z^*(\to \tau^+\tau^-)$

We begin our discussion by presenting an explicit form of the three-fold angular decay distribution given by Eq. (8). The relevant helicity components of the on-shell and off-shell lepton tensors are listed in Appendix B while the helicity components of the $H \to ZZ^*$ transition amplitude can be found in Appendix A. The polar angles θ_p and θ_q are defined in the respective lepton pair center-of-mass systems as shown in Fig. 1. The azimuthal angle χ describes the relative orientation of the two decay planes. We split the decay distribution into a helicity-nonflip and helicity-flip part,

$$
\begin{aligned}
(2p^2 2q^2)^{-1}\, W^Z_{nf}(\theta_p,\theta_q,\chi) \;=\; & (\rho_{++}+\rho_{--}) \\
& \times \Big(\tfrac{1}{4}(1+\cos^2\theta_p)(v_\ell^2+a_\ell^2 v_p^2)(1+\cos^2\theta_q)(v_\ell^2+a_\ell^2 v_q^2) + 4\cos\theta_p\cos\theta_q v_\ell^2 a_\ell^2 v_p v_q\Big) \\
& + \rho_{00}\sin^2\theta_p(v_\ell^2+a_\ell^2 v_p^2)\sin^2\theta_q(v_\ell^2+a_\ell^2 v_q^2) + (\rho_{++}-\rho_{--}) \\
& \times \Big((1+\cos^2\theta_p)(v_\ell^2+a_\ell^2 v_p^2)\cos\theta_q v_q + \cos\theta_p v_p(1+\cos^2\theta_q)(v_\ell^2+a_\ell^2 v_q^2)\Big)\, v_\ell a_\ell \\
& + (\rho_{+0}+\rho_{-0})\sin\theta_p\sin\theta_q\Big(4v_\ell^2 a_\ell^2 v_p v_q + \cos\theta_p(v_\ell^2+a_\ell^2 v_p^2)\cos\theta_q(v_\ell^2+a_\ell^2 v_q^2)\Big)\cos\chi \\
& + 2(\rho_{+0}-\rho_{-0})\sin\theta_p\sin\theta_q v_\ell a_\ell\Big(\cos\theta_p(v_\ell^2+a_\ell^2 v_p^2)v_q + \cos\theta_q(v_\ell^2+a_\ell^2 v_q^2)v_p\Big)\cos\chi \\
& + \tfrac{1}{2}\rho_{+-}\sin^2\theta_p(v_\ell^2+a_\ell^2 v_p^2)\sin^2\theta_q(v_\ell^2+a_\ell^2 v_q^2)\cos 2\chi
\end{aligned}
\tag{9}
$$

and

$$
\begin{aligned}
(2p^2 2q^2)^{-1}\, W^Z_{hf}(\theta_p,\theta_q,\chi) \;=\; & \frac{4m_\tau^2}{q^2}\Big\{(v_\ell^2+a_\ell^2 v_p^2)\,\times \\
& \Big(\tfrac{1}{4}(\rho_{++}+\rho_{--})(1+\cos^2\theta_p)\sin^2\theta_q v_\ell^2 + \rho_{00}\sin^2\theta_p\cos^2\theta_q v_\ell^2 + \rho_S\, F_S^2\sin^2\theta_p a_\ell^2 \\
& - \tfrac{1}{4}(\rho_{+0}+\rho_{-0})\sin 2\theta_p \sin 2\theta_q v_\ell^2\cos\chi - \tfrac{1}{2}\rho_{+-}\sin^2\theta_p\sin^2\theta_q v_\ell^2\cos 2\chi\Big) \\
& + (\rho_{++}-\rho_{--})\cos\theta_p v_p \sin^2\theta_q v_\ell^3 a_\ell - (\rho_{+0}-\rho_{-0})\sin\theta_p v_p \sin 2\theta_q v_\ell^3 a_\ell\cos\chi\Big\}, \qquad (10)
\end{aligned}
$$

where $v_p^2 = 1 - 4m_{\ell p}^2/p^2$ and $v_q^2 = 1 - 4m_{\ell q}^2/q^2$. For symmetry reasons and for later applications in the off-shell – off-shell case we have written p^2 for m_Z^2 and $v_p^2 = 1 - 4m_{\ell p}^2/p^2$ for $v_p^2 = 1$ on the on-shell side. The double spin-density matrix elements $\rho_{mm'}$ are bilinear forms of the helicity amplitudes describing the $H \to ZZ^*$ transitions. They are defined in Appendix A.

In Eqs. (9) and (10) we have also included the contributions from the parity-violating terms proportional to $(\rho_{++} - \rho_{--})$ and $(\rho_{+0} - \rho_{-0})$. These coefficient functions are not populated by the parity-conserving SM (HVV) coupling. In Appendix A we briefly discuss the contribution of a parity-violating non-SM coupling proportional to $\epsilon^{\mu\nu\rho\sigma}p_\rho q_\sigma$ which would populate the $(\rho_{++} - \rho_{--})$ and $(\rho_{+0} - \rho_{-0})$ coefficient functions [17, 18, 19].

We add the flip and non-flip contributions and expand the result in terms of the Legendre polynomials $P_1(\cos\theta) = \cos\theta$ and $P_2(\cos\theta) = \frac{1}{2}(3\cos^2\theta - 1)$. The result is written in the form

$$
(2p^2 2q^2)^{-1}\, W^Z(\theta_p,\theta_q,\chi) = \frac{4}{9}\sum_{i=0}^{7}\mathcal{F}_i^Z h_i(\theta_p,\theta_q,\chi) = \frac{4}{9}\sum_{i=0}^{7}\Big(f_i^Z + \varepsilon g_i^Z\Big)h_i(\theta_p,\theta_q,\chi), \qquad (11)
$$

where in the second equation of (11) we have split the coefficient function $\mathcal{F}_i^Z$ into its helicity-flip and helicity-nonflip part using the notation $\varepsilon = m_\tau^2/q^2$.

The coefficient functions f_i^Z and g_i^Z and their associated angular factors $h_i(\theta_p,\theta_q,\chi)$ are listed in Table 1 where we use the abbreviation $C_{ew}^{(i)} = v_\ell^2 + a_\ell^2 v_i^2$ with $i = p, q$. In addition we use a short-hand notation for the double density matrix elements, namely $\rho_U = \rho_{++} + \rho_{--}$, $\rho_L = \rho_{00}$, $\rho_{U+L} = \rho_U + \rho_L$ and $\rho_S = \rho_{tt}$. Note that we have dropped the

i	f_i^Z	g_i^Z	$h_i(\theta_p, \theta_q, \chi)$
0	$C_{ew}^{(p)} C_{ew}^{(q)}\, \rho_{U+L}$	$2C_{ew}^{(p)}(v_\ell^2 \rho_{U+L} + 3a_\ell^2 F_S^2 \rho_S)$	1
1	$\frac{1}{2} C_{ew}^{(p)} C_{ew}^{(q)} (\rho_U - 2\rho_L)$	$-2C_{ew}^{(p)} v_\ell^2 (\rho_U - 2\rho_L)$	$P_2(\cos\theta_q)$
2	$\frac{1}{2} C_{ew}^{(p)} C_{ew}^{(q)} (\rho_U - 2\rho_L)$	$C_{ew}^{(p)} \left(v_\ell^2 (\rho_U - 2\rho_L) - 6a_\ell^2 F_S^2 \rho_S \right)$	$P_2(\cos\theta_p)$
3	$\frac{1}{4} C_{ew}^{(p)} C_{ew}^{(q)} (\rho_U + 4\rho_L)$	$-C_{ew}^{(p)} v_\ell^2 (\rho_U + 4\rho_L)$	$P_2(\cos\theta_p) P_2(\cos\theta_q)$
4	$9 v_\ell^2 a_\ell^2 v_p v_q \rho_U$	0	$\cos\theta_p \cos\theta_q$
5	$9 v_\ell^2 a_\ell^2 v_p v_q (\rho_{+0} + \rho_{-0})$	0	$\sin\theta_p \sin\theta_q \cos\chi$
6	$\frac{9}{16} C_{ew}^{(p)} C_{ew}^{(q)} (\rho_{+0} + \rho_{-0})$	$-\frac{9}{4} C_{ew}^{(p)} v_\ell^2 (\rho_{+0} + \rho_{-0})$	$\sin 2\theta_p \sin 2\theta_q \cos\chi$
7	$\frac{9}{8} C_{ew}^{(p)} C_{ew}^{(q)} \rho_{+-}$	$-\frac{9}{2} C_{ew}^{(p)} v_\ell^2 \rho_{+-}$	$\sin^2\theta_p \sin^2\theta_q \cos 2\chi$

Table 1: Coefficient functions appearing in the three-fold angular decay distribution of the decay $H \to Z^{*0}(\to \ell^+\ell^-) + Z^*(\to \tau^+\tau^-)$

contributions of the parity-violating terms proportional to $(\rho_{++} - \rho_{--})$ and $(\rho_{+0} - \rho_{-0})$ in Table 1 which are not populated by the parity-conserving SM (HVV) coupling.

The dominant flip contributions proportional to a_ℓ^2 are contained in g_0^Z and g_2^Z. Compared to a_ℓ the leptonic vector coupling $v_\ell = -1 + \sin^2\theta_W$ is much suppressed. This is different in the quark–antiquark case treated in Refs. [36, 37] where the electroweak vector and axial vector couplings to the quark pairs are comparable in size. As a result the pattern of the helicity-flip contributions in the quark pair production case is quite different from the lepton-pair production case [36, 37].

In order to save space we have not expanded the angular factor $\sin^2\theta_p \sin^2\theta_q$ in the last row of Table 1. The relevant expansion would be given by

$$\sin^2\theta_p \sin^2\theta_q = \frac{4}{9}\Big(1 - P_2(\cos\theta_p) - P_2(\cos\theta_q) + P_2(\cos\theta_p) P_2(\cos\theta_q)\Big). \qquad (12)$$

We then define a normalized decay distribution

$$\widetilde{W}^Z(\theta_p,\theta_q,\chi)=\frac{W^Z(\theta_p,\theta_q,\chi)}{\int W^Z(\theta'_p,\theta'_q,\chi')d\cos\theta'_p\,d\cos\theta'_q\,d\chi'}=\frac{1}{8\pi}\Big(1+\sum_{i=1}^{7}\widetilde{\mathcal{F}}_i^Z h_i(\theta_p,\theta_q,\chi)\Big), \quad (13)$$

where $\widetilde{\mathcal{F}}_i^Z=\mathcal{F}_i^Z/\mathcal{F}_0^Z$ (and $\tilde{f}_i^Z=f_i^Z/\mathcal{F}_0^Z$, $\tilde{g}_i^Z=g_i^Z/\mathcal{F}_0^Z$) and where

$$\mathcal{F}_0^Z=f_0^Z+\varepsilon g_0^Z=C_{ew}^{(p)}C_{ew}^{(q)}\rho_{U+L}+2\varepsilon C_{ew}^{(p)}(v_\ell^2\rho_{U+L}+3a_\ell^2F_S^2\rho_S). \quad (14)$$

The normalized angular decay distribution $\widetilde{W}^Z(\theta_p,\theta_q,\chi)$ obviously integrates to 1, i.e.

$$\int\widetilde{W}^Z(\theta_p,\theta_q,\chi)\,d\cos\theta_p\,d\cos\theta_q\,d\chi\;=\;1. \quad (15)$$

Before we start discussing our numerical results we want to specify our mass, width and coupling input parameters. We use the central value of the Higgs mass $m_H=125.09(24)\,\text{GeV}$ from the combined ATLAS and CMS measurement [38]. For the remaining parameters we use the central values from the PDG [39] given by

$$\begin{aligned} m_W&=80.385(15)\,\text{GeV}, & \Gamma_W&=2.085(42)\,\text{GeV},\\ m_Z&=91.1876(21)\,\text{GeV}, & \Gamma_Z&=2.4952(23)\,\text{GeV},\\ m_\tau&=1.77682(16)\,\text{GeV},\\ \sin^2\theta_W&=0.23126(5), & G_F&=1.1663787(6)\times10^{-5}\,\text{GeV}^{-2}. \end{aligned} \quad (16)$$

Our formulas are written in terms of the dimensionless coupling constant g^2 which is related to G_F by $g^2=8m_W^2G_F/\sqrt{2}$. For practical numerical purposes we choose $m_{\ell p}=m_e$ (or $m_{\ell p}=0$) on the p side. On the off-shell q side we write $m_{\ell q}=m_\ell$ which can take the values $m_\ell=m_\tau$ or $m_\ell=m_{e,\mu}$.

In Table 2 we present numerical results for the normalized coefficient functions $\widetilde{\mathcal{F}}_i^Z(q^2)$ and their averages. In columns 2 and 3 we list the values of $\widetilde{\mathcal{F}}_i^Z(q^2)$ for $q^2=50\,\text{GeV}^2$ with zero and nonzero lepton masses. In order to avoid possible contamination from contributions of the ψ and Υ families we have chosen a q^2 value in between these two families, namely $q^2=50\,\text{GeV}^2$. This q^2 value is small enough to highlight the helicity-flip

i	$\widetilde{\mathcal{F}}_i^Z\ (m_\ell = 0)$	$\widetilde{\mathcal{F}}_i^Z\ (m_\ell = m_\tau)$	$\langle\widetilde{\mathcal{F}}_i^Z\rangle\ (m_\ell = 0)$	$\langle\widetilde{\mathcal{F}}_i^Z\rangle\ (m_\ell = m_\tau)$
1	-0.9115	-0.6257	-0.3916	-0.3491
2	-0.9115	-0.9391	-0.3916	-0.3908
3	$+0.9557$	$+0.6561$	$+0.6958$	$+0.6537$
4	$+0.0030$	$+0.0023$	$+0.0203$	$+0.0206$
5	$+0.0167$	$+0.0132$	$+0.0319$	$+0.0319$
6	$+0.1875$	$+0.1287$	$+0.3589$	$+0.3528$
7	$+0.0332$	$+0.0228$	$+0.2281$	$+0.2284$

Table 2: Numerical results for the normalized coefficient functions $\widetilde{\mathcal{F}}_i^Z(q^2)$ at $q^2 = 50\,\mathrm{GeV}^2$ and the average of $\widetilde{\mathcal{F}}_i^Z(q^2)$ over $q^2 \in [4m_\ell^2, (m_H - m_Z)^2]$

and lepton-mass effects in the vicinity of the threshold. On the other hand, this value of q^2 is far away enough from the threshold region where one would have to deal with the Coulomb singularity. We mention that the contribution of the ψ and Υ families to the q^2 spectrum have been investigated in Ref. [40]. These contributions have been found to be small.

Concerning the $q^2 = 50\,\mathrm{GeV}^2$ values for the normalized coefficient functions, lepton-mass effects amount to $-31\,\%$ for the functions $\widetilde{\mathcal{F}}_{1,3,6,7}^Z$, $-21\,\%$ for the functions $\widetilde{\mathcal{F}}_{4,5}^Z$, and $+3\,\%$ for the function $\widetilde{\mathcal{F}}_2^Z$. The normalized coefficient functions $\widetilde{\mathcal{F}}_{6,7}^Z$ are quite small to start with. We mention that τ-lepton mass effects are even larger for smaller values of q^2.

In columns 4 and 5 of Table 2 we also present average values $\langle\widetilde{\mathcal{F}}_i^Z\rangle$ of the coefficient functions again for zero and nonzero lepton masses where the average is taken with regard to q^2. In order to do the requisite q^2 integrations one needs to include the relevant q^2-dependent integration measure defined by the differential q^2 distribution. Inserting the

necessary coupling and phase-space factors one obtains

$$\frac{d\Gamma^Z}{dq^2\, d\cos\theta_p\, d\cos\theta_q\, d\chi} = \frac{B_{Z\ell\ell}}{C_{ew}^{(p)}}\,\frac{C^Z(q^2)}{8\pi} \times \frac{9}{4} W^Z(q^2,\theta_p,\theta_q,\chi), \tag{17}$$

where

$$C^Z(q^2) = \frac{g^4}{\cos^4\theta_W}\,\frac{1}{4\cdot 1536\pi^3}\,\frac{|\vec{p}_V(m_Z^2,q^2)|v_q}{m_H^2}\,\frac{1}{(q^2-m_Z^2)^2+m_Z^2\Gamma_Z^2}\,. \tag{18}$$

$B_{Z\ell\ell}$ is the branching ratio of the decay $Z\to\ell^+\ell^-$, i.e. $B_{Z\ell\ell}=\Gamma(Z\to\ell^+\ell^-)/\Gamma(Z)$, where the rate for the decay $Z\to\ell^+\ell^-$ $(m_{\ell p}=0)$ reads

$$\Gamma_{Z\ell\ell} = \Gamma(Z\to\ell^+\ell^-) = \frac{g^2}{\cos^2\theta_W}\,\frac{1}{192\pi} m_Z\,(v_\ell^2+a_\ell^2). \tag{19}$$

The magnitude of the momentum of the gauge bosons is given by

$$|\vec{p}_V(p^2,q^2)| = \frac{1}{2m_H}\sqrt{\lambda(m_H^2,p^2,q^2)}, \tag{20}$$

where $\lambda(a,b,c)=a^2+b^2+c^2-2ab-2ac-2bc$ is Källén's function. We then define partial differential rates according to

$$\frac{d\,\Gamma_i^Z}{dq^2} = 2p^2\,2q^2\frac{B_{Z\ell\ell}C^Z(q^2)}{C_{ew}^{(p)}}\mathcal{F}_i^Z(q^2). \tag{21}$$

The factors $p^2=m_Z^2$ and q^2 are picked up when doing the integrations over the $Z\to\ell^+\ell^-$ and $Z^*\to\ell^+\ell^-$ phase spaces. The factor q^2 is of crucial importance to cancel the $1/q^2$ singularity in the double spin-density matrix elements ρ_{00}, ρ_{0t} and ρ_{tt} at the lower end of the q^2 spectrum. The average values of the coefficient functions $\langle\widetilde{\mathcal{F}}_i^Z\rangle$ can be calculated from the formula

$$\langle\widetilde{\mathcal{F}}_i^Z\rangle = \frac{\int dq^2 2p^2 2q^2 B_{Z\ell\ell}C^Z(q^2)\mathcal{F}_i^Z(q^2)/C_{ew}^{(p)}}{\int dq^2 2p^2 2q^2 B_{Z\ell\ell}C^Z(q^2)\mathcal{F}_0^Z(q^2)/C_{ew}^{(p)}} = \frac{\Gamma_i^Z}{\Gamma^Z}. \tag{22}$$

The integration has to be done in the limits $4m_\ell^2\le q^2\le(m_H-m_Z)^2$. The denominator of Eq. (22) is nothing but the total rate Γ^Z including lepton mass effects. When calculating the average values according to Eq. (22) one can disregard all constant factors in the weight function $C^Z(q^2)$.

Numerically, one finds that the averaged coefficient function $\langle\widetilde{\mathcal{F}}_3^Z\rangle$ is by far the largest one. Lepton-mass effects are largest for $\langle\widetilde{\mathcal{F}}_{1,3}^Z\rangle$ and amount to $-10.8\,\%$ and $-6.1\,\%$.

Using the average values $\langle\widetilde{\mathcal{F}}_i^Z\rangle$, the q^2-integrated angular decay distribution can be written as

$$\frac{1}{\Gamma^Z}\frac{d\,\Gamma^Z}{d\cos\theta_p\,d\cos\theta_q\,d\chi} = \frac{1}{8\pi}\Big(1+\sum_{i=1}^{7}\langle\widetilde{\mathcal{F}}_i^Z\rangle\,h_i(\theta_p,\theta_q,\chi)\Big). \tag{23}$$

One can make contact with the work of Ref. [41] by taking the zero-mass limit $m_{\ell q}\to 0$ of Eq. (21) (for $i=0$), neglecting the Z width and omitting the factor $B_{Z\ell\ell}$. In fact, using the notation $\hat{m}_Z = m_Z/m_H$ and $\hat{q}^2 = q^2/m_H^2$ one obtains

$$\frac{d\Gamma^Z}{d\hat{q}^2} = \frac{g^4}{\cos^4\theta_W}\frac{m_H C_{ew}^{(q)}}{4\cdot 3072\pi^3}\lambda^{1/2}(1,\hat{m}_Z^2,\hat{q}^2)\;\frac{\hat{q}^4+\hat{q}^2(10\hat{m}_Z^2-2)+(1-\hat{m}_Z^2)^2}{(\hat{q}^2-\hat{m}_Z^2)^2} \tag{24}$$

in agreement with Refs. [41, 42]. At $\hat{q}^2=0$ one has

$$\frac{d\Gamma^Z}{d\hat{q}^2}(\hat{q}^2=0) = \frac{g^4}{\cos^4\theta_W}\frac{m_H C_{ew}^{(q)}}{4\cdot 3072\pi^3}\frac{(1-\hat{m}_Z^2)^3}{\hat{m}_Z^4} = 4.02\cdot 10^{-2}\,\text{MeV}. \tag{25}$$

Integrating Eq. (24) within the limits $0\le\hat{q}^2\le(1-\hat{m}_Z)^2$ one obtains the well-known expression [41, 42]

$$\Gamma(H\to Z\,\ell^+\ell^-) = \frac{g^4}{\cos^4\theta_W}\frac{m_H}{4\cdot 3072\pi^3}F(\hat{m}_Z) \tag{26}$$

with

$$\begin{aligned} F(\hat{m}_Z) \;=\; & \frac{3(1-8\hat{m}_Z^2+20\hat{m}_Z^4)}{(4\hat{m}_Z^2-1)^{1/2}}\arccos\Big(\frac{3\hat{m}_Z^2-1}{2\hat{m}_Z^3}\Big) \\ & -(1-\hat{m}_Z^2)\Big(\frac{47}{2}\hat{m}_Z^2-\frac{13}{2}+\frac{1}{\hat{m}_Z^2}\Big)-3(1-6\hat{m}_Z^2+4\hat{m}_Z^4)\ln\hat{m}_Z. \end{aligned} \tag{27}$$

3.2 Single-angle decay distributions

Integrating Eq. (13) over $\cos\theta_p$ and χ and using Table 1, one obtains

$$\widetilde{W}^Z(q^2,\theta_q) = \frac{1}{2}\left(1+\widetilde{\mathcal{F}}_1^Z P_2(\cos\theta_q)\right). \tag{28}$$

We define a convexity parameter $C_f^{(q)}(q^2)$ as the second derivative of Eq. (28) with respect to $\cos\theta_q$ or, equivalently, as two times the coefficient of the $\cos^2\theta_q$ term in Eq. (28). One

obtains

$$C_f^{(q)}(q^2) = \frac{3}{2}\,\widetilde{\mathcal{F}}_1^Z = \frac{3}{2}\,\frac{f_1^Z + \varepsilon g_1^Z}{f_0^Z + \varepsilon g_0^Z} = \frac{3}{4}\,\frac{\rho_U - 2\rho_L}{\rho_{U+L}}\,\frac{(q^2-4m_\ell^2)(v_\ell^2+a_\ell^2)}{C_{ew}^{(q)} q^2 + 2m_\ell^2(v_\ell^2 + 3a_\ell^2 F_S^2 \rho_S/\rho_{U+L})}. \quad (29)$$

In Fig. 2 we show a plot of the q^2 distribution of the convexity parameter for both the $m_\ell = 0$ and $m_\ell = m_\tau$ cases. Due to the overall factor $(q^2 - 4m_\ell^2)$ one has $C_f^{(q)}(q^2) \to 0$ at threshold (maximal recoil) $q^2 = 4m_\ell^2$, i.e. the $\cos^2\theta_q$ distribution is flat at threshold. This is clearly visible in the $\ell = \tau$ case in Fig. 2. For $\ell = e, \mu$ the vanishing of the convexity parameter $C_f^{(q)}(q^2)$ at threshold is not discernible at the scale of Fig. 2. Instead $C_f^{(q)}(q^2) \to -3/2$ at threshold as $m_\ell^2 \to 0$ due to the limiting behaviour of the two factors in Eq. (29). The first factor goes to $-3/2$ because of the dominance of ρ_L and the second factor goes to 1 in this limit. A closer look at the second factor in Eq. (29) reveals that it shows a steplike behaviour at threshold for $m_\ell \to 0$ jumping from 0 to 1. In fact, setting $F_S^2\,\rho_S/\rho_{U+L} \sim 1$ in the second factor in Eq. (29) one obtains the limiting form

$$\frac{(q^2-4m_\ell^2)(v_\ell^2+a_\ell^2)}{C_{ew}^{(q)} q^2 + 2m_\ell^2(v_\ell^2 + 3a_\ell^2 F_S^2 \rho_S/\rho_{U+L})} \quad \to \quad (q^2-4m_\ell^2)/(q^2+2m_\ell^2)\,. \quad (30)$$

Equation (30) shows the advertised steplike behaviour as $m_\ell^2 \to 0$. Even for the muon the deviation from 1 at $q^2 = 10\,\mathrm{GeV}^2$ is a tiny one (0.67 %). At the other end of the spectrum at minimal (zero) recoil where $q^2 = (m_H - m_Z)^2$ the convexity parameter goes to zero in both cases since $\rho_U - 2\rho_L \sim |\vec{q}|^2$ and $|\vec{q}| = 0$ at zero recoil.

Figure 2 shows that the convexity parameter $C_f^{(q)}$ is negative, i.e. the polar angle distribution is described by a downward-open parabola which has a maximum at $\cos\theta_q = 0$ with the maximal value $\widetilde{W}^Z(q^2, \theta_q = \pi/2) = \frac{1}{2}(1 - C_f^{(q)}(q^2)/3)$. In Fig. 3 we show a plot of the $\cos\theta_q$ distribution for $q^2 = 50\,\mathrm{GeV}^2$. The $\cos\theta_q$ distribution is symmetric in $\cos\theta_q$ due to the absence of a term linear in $\cos\theta_q$ in Eq.(28), i.e. the distribution is forward–backward symmetric. As expected from Eq. (30) the $m_\ell = m_\tau$ curve is considerably flatter than the $m_\ell = 0$ curve. At $\cos\theta_q = \pm 1$ the $m_\ell = 0$ curve is close to zero since $P_2(\cos\theta_q) = 1$ at these points and $\widetilde{\mathcal{F}}_2^Z = f_1^Z/f_0^Z \approx -1$ due to the dominance of the longitudinal contribution ρ_L.

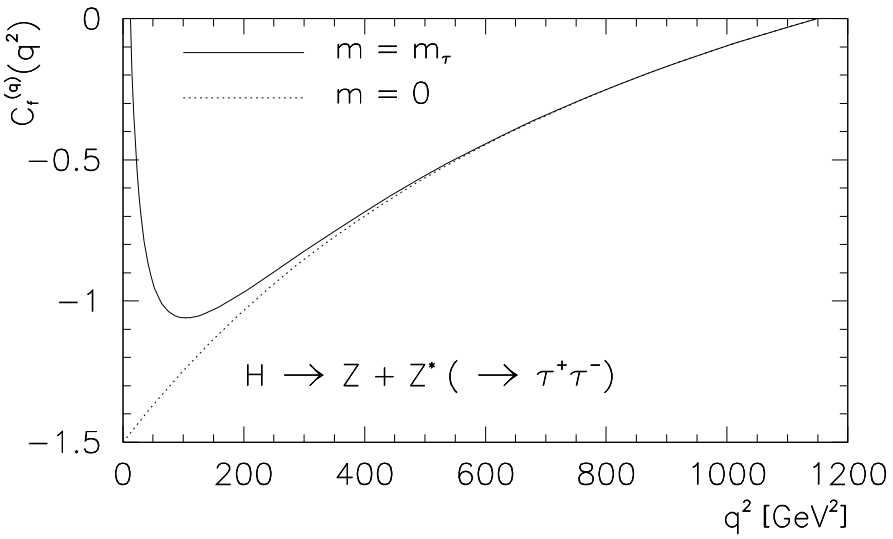


Figure 2: q^2 distribution of the convexity parameter for $m_\ell = 0$ (dotted line) and $m_\ell = m_\tau$ (solid line) for the process $H \to Z + Z^*(\to \ell^+\ell^-)$

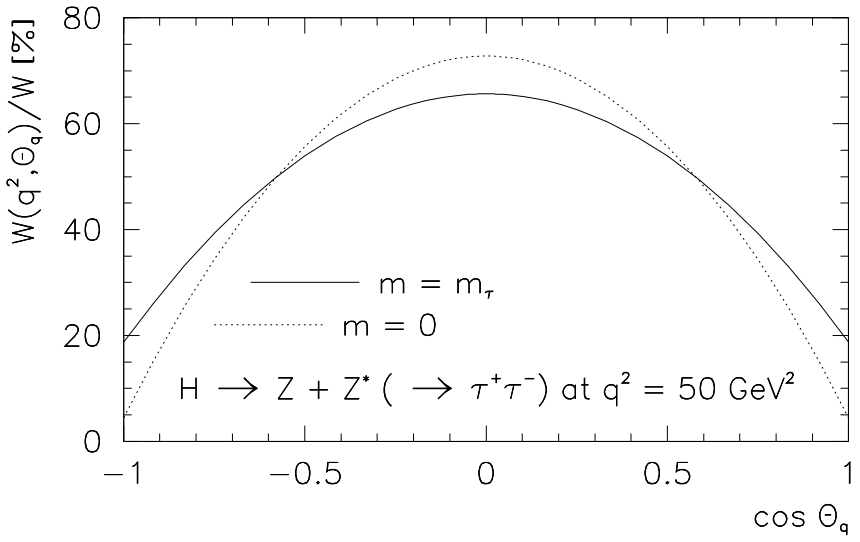


Figure 3: $\cos\theta_q$ dependence of the normalized decay distribution $\widetilde{W}^Z(q^2, \theta_q)$ for $q^2 = 50\,\mathrm{GeV}^2$ in case of $m_\ell = 0$ (dotted line) and $m_\ell = m_\tau$ (solid line)

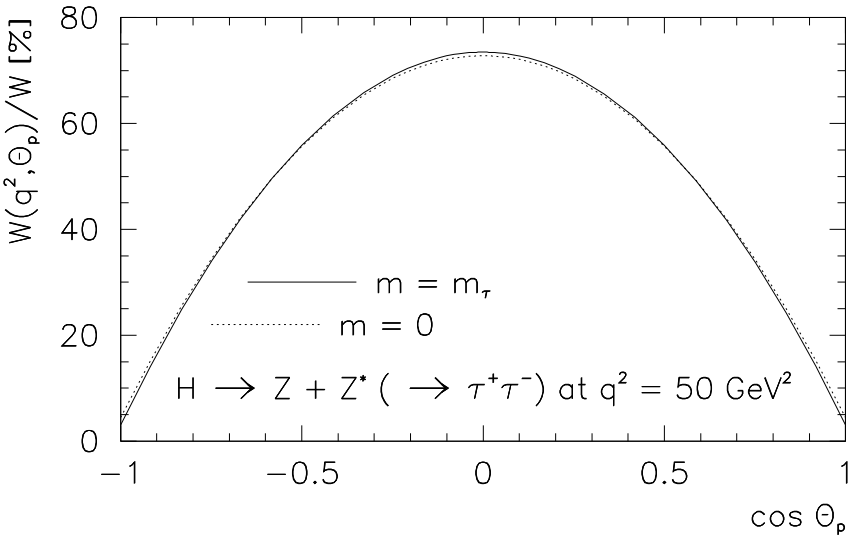


Figure 4: $\cos\theta_p$ dependence of the normalized decay distribution $\widetilde{W}^Z(q^2,\theta_p)$ for $q^2 = 50\,\mathrm{GeV}^2$ in case of $m_\ell = 0$ (dotted line) and $m_\ell = m_\tau$ (solid line)

Next we discuss the single-angle $\cos\theta_p$ distribution. From Table 1 one reads off

$$\widetilde{W}^Z(q^2,\theta_p) = \frac{1}{2}\left(1 + \widetilde{\mathcal{F}}_2^Z P_2(\cos\theta_p)\right). \tag{31}$$

The corresponding convexity factor is now given by

$$C_f^{(p)}(q^2) = \frac{3}{2}\,\widetilde{\mathcal{F}}_2^Z = \frac{3}{2}\,\frac{f_2^Z + \varepsilon g_2^Z}{f_0^Z + \varepsilon g_0^Z} = \frac{3}{4}\,\frac{\rho_U - 2\rho_L}{\rho_{U+L}}\,\frac{C_{ew}^{(q)} q^2 + 2m_\ell^2(v_\ell^2 - 6a_\ell^2 F_S^2\rho_S/\rho_{U-2L})}{C_{ew}^{(q)} q^2 + 2m_\ell^2(v_\ell^2 + 3a_\ell^2 F_S^2\rho_S/\rho_{U+L})}. \tag{32}$$

The threshold value of the convexity parameter can now be seen to be given by $C_f^{(p)}(q^2) = -3/2$ in both the $m_\ell = 0$ and $m_\ell = m_\tau$ cases. We do not provide a plot of the convexity parameter $C_f^{(p)}(q^2)$ because lepton-mass effects are small even close to threshold. In Fig. 4 we plot the $\cos\theta_p$ dependence of the normalized single-angle distribution again for $q^2 = 50\,\mathrm{GeV}^2$. There is practically no lepton-mass dependence in the $\cos\theta_p$ distribution. Since $\widetilde{\mathcal{F}}_2^Z = \widetilde{\mathcal{F}}_1^Z$ in the zero mass case, the zero lepton-mass distributions in Figs. 3 and 4 are identical to each other.

Finally we turn to the normalized single-angle azimuthal distribution, where

$$\widetilde{W}^Z(\chi) = \frac{1}{2\pi}\left(1 + \frac{\pi^2}{16}\widetilde{\mathcal{F}}_5^Z\cos\chi + \frac{4}{9}\widetilde{\mathcal{F}}_7^Z\cos 2\chi\right). \tag{33}$$

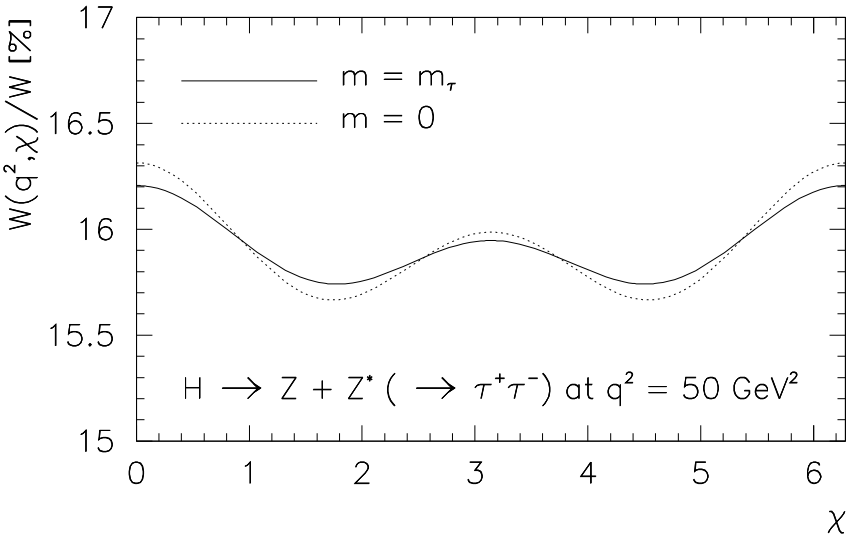


Figure 5: χ dependence of the normalized decay distribution $\widetilde{W}^Z(q^2,\chi)$ for $q^2 = 50\,\mathrm{GeV}^2$ in case of $m_\ell = 0$ (dotted line) and $m_\ell = m_\tau$ (solid line)

In Fig. 5 we show the χ dependence of $\widetilde{W}^Z(q^2,\chi)$ again for $q^2 = 50\,\mathrm{GeV}^2$. The nonflip contribution to the coefficient of the $\cos 2\chi$ term clearly dominates the decay distribution since the leading contribution is given by $f_7^Z \sim a_\ell^2 v_q^2 \rho_{+-} = a_\ell^2 v_q^2$. The dominance of the $\cos 2\chi$ term is clearly evident in Fig. 5. Lepton-mass effects are generally small and amount to maximally $\sim 1.2\,\%$ at $\chi = 0,\ \pi/2,\ 3/2\pi,\ 2\pi$ where the mass dependence mainly results from the normalization.

3.3 The polarization of the off-shell gauge boson Z^*

In Sec. 3.2 we have already considered the single-angle $\cos\theta_q$ distribution which we wrote in the form $\sim (1 + \widetilde{\mathcal{F}}_1^Z P_2(\cos\theta_q))$. In this subsection we want to write the same angular decay distribution in terms of the transverse, longitudinal and scalar components ρ_U, ρ_L and ρ_S of the double spin-density matrix $\rho_{mm'}$. One obtains

$$\frac{d\Gamma^Z}{dq^2 d\cos\theta_q} \;=\; 2p^2 2q^2 B_{Z\ell\ell} C^Z(q^2) \Bigg\{ \left[\frac{3}{8}(1+\cos^2\theta_q)\,\rho_U + \frac{3}{4}\sin^2\theta_q\,\rho_L\right] C_{ew}^{(q)}$$

$$
\begin{aligned}
&+\frac{2m_\ell^2}{q^2}\left[\left(\frac{3}{4}\sin^2\theta_q\,\rho_U+\frac{3}{2}\cos^2\theta_q\,\rho_L\right)v_\ell^2+\frac{3}{2}F_S^2(q^2)\rho_S a_\ell^2\right]\Bigg\}\\
=\;& 2p^2 2q^2 B_{Z\ell\ell}C^Z(q^2)\Bigg\{\left[\frac{3}{8}(1+\cos^2\theta_q)\rho_U+\frac{3}{4}\sin^2\theta_q\,\rho_L\right]\left(C_{ew}^{(q)}-4\varepsilon v_\ell^2\right)\\
&+3\varepsilon\Big(\rho_{U+L}v_\ell^2+F_S^2(q^2)\rho_S a_\ell^2\Big)\Bigg\}. \qquad (34)
\end{aligned}
$$

Integrating the differential rate (34) with respect to $\cos\theta_q$, one obtains

$$
\frac{d\Gamma^Z}{dq^2}=2p^2 2q^2 B_{Z\ell\ell}C^Z(q^2)\Bigg\{\left(C_{ew}^{(q)}+\frac{2m_\ell^2}{q^2}v_\ell^2\right)(\rho_U+\rho_L)+\frac{6m_\ell^2}{q^2}F_S^2(q^2)a_\ell^2\rho_S\Bigg\}. \qquad (35)
$$

Equation (35) can be seen to be the equivalent of the $i=0$ piece of Eq. (21). Accordingly we define partial rates by writing

$$
\begin{aligned}
\frac{d\Gamma_{U,L}^Z}{dq^2} &= 2p^2 2q^2 B_{Z\ell\ell}C^Z(q^2)\left(C_{ew}^{(q)}+\frac{2m_\ell^2}{q^2}v_\ell^2\right)\rho_{U,L}\,,\\
\frac{d\Gamma_S^Z}{dq^2} &= 2p^2 2q^2 B_{Z\ell\ell}C^Z(q^2)\frac{6m_\ell^2}{q^2}F_S^2(q^2)a_\ell^2\rho_S. \qquad (36)
\end{aligned}
$$

In Fig. 6 we display the q^2 dependence of the three partial rates $d\Gamma_\alpha^Z/dq^2$ ($\alpha=U,L,S$) for the two cases $m_\ell=0$ and $m_\ell=m_\tau$. Lepton mass effects are largest for q^2 values in the vicinity of the threshold. There is a substantial tauonic scalar rate for low q^2 values which partially compensates for the loss of longitudinal rate in the low q^2 region. In the massless case, where there is no scalar partial rate, the longitudinal rate dominates the transverse rate up to $\sim 700\,\mathrm{GeV}^2$. The transverse rate $d\Gamma_U^Z/dq^2$ shows a very small lepton-mass dependence. The transverse rates vanish at threshold due to their respective threshold factors. The $q^2=0$ mass-zero rate can be seen to be in numerical agreement with the corresponding $q^2=0$ value of Ref. [41] listed in Eq. (25).

The angular decay distributions are given by the normalized partial rates $d\Gamma_{U,L,S}/dq^2$ divided by the total rate $d\Gamma_{U+L+S}/dq^2$. For brevity we denote these normalized rates by $\widetilde{U}$, $\widetilde{L}$ and $\widetilde{S}$. Again we take our reference value $q^2=50\,\mathrm{GeV}^2$. The transverse–longitudinal–scalar helicity fractions are given by

$$
\widetilde{U}\,:\,\widetilde{L}\,:\,\widetilde{S}=0.06\,:\,0.94\,:\,0 \qquad\qquad \widetilde{U}\,:\,\widetilde{L}\,:\,\widetilde{S}=0.04\,:\,0.65\,:\,0.31. \qquad (37)
$$

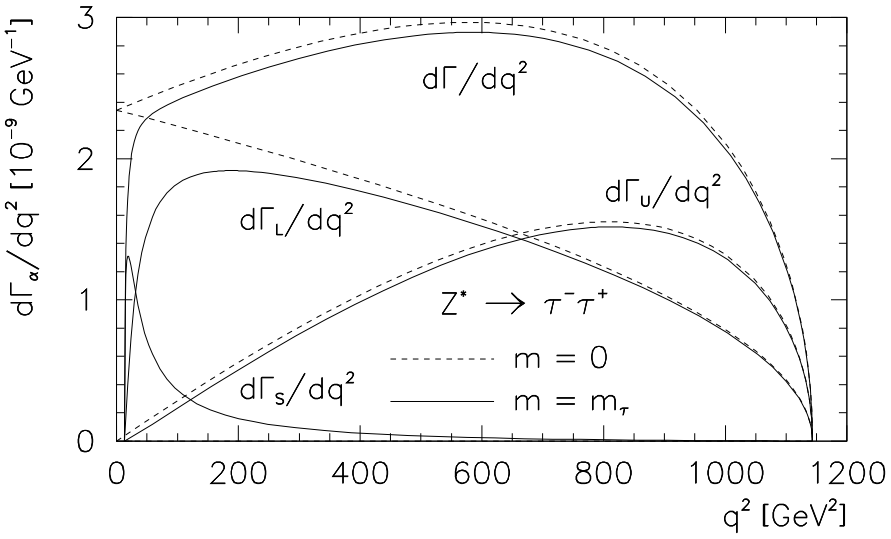


Figure 6: Differential rates $d\Gamma_\alpha^Z/dq^2$ (indices $\alpha = U, L, S$ and vanishing index for $\alpha = U+L$) for the decay $H \to Z(\to e^+e^-) + Z^*(\to \ell^+\ell^-)$ with $m_\ell = 0$ and $m_\ell = m_\tau$

The left and right three values refer to the modes $H \to Z(\to e^+e^-) + Z^*(\to \mu^+\mu^-)$ and $H \to Z(\to e^+e^-) + Z^*(\to \tau^+\tau^-)$, respectively. In the τ mode one observes a substantial loss in the longitudinal rate which is compensated for by the appearance of the scalar rate. This has consequences for the $\cos\theta_q$ distribution as shown in Fig. 3.

In the upper part of Table 3 we list the total rate and the mean values of the transverse, longitudinal and scalar partial rates for the mass-zero modes and the τ mode where the mean is taken with regard to q^2. Lepton-mass effects reduce the total rate by 3.97 %. The rate reduction is largest for the longitudinal rate where the rate reduction amounts to 6.99 %. This is partially made up for by the appearance of the scalar rate which amounts to 4.14 %. The average transverse rate is practically unaffected by lepton mass effects.

3.4 Off-shell – off-shell decays $H \to Z^*(\to \ell^+\ell^-) + Z^*(\to \tau^+\tau^-)$

To conclude the section about Higgs boson decays into a pair of Z bosons, we briefly consider the case where both Z bosons are off-shell. The double-differential decay rate for

$H \to Z^*(\to \ell_p^+\ell_p^-)\, Z^*(\to \ell_q^+\ell_q^-)$ reads $(\ell_p \neq \ell_q)$

$$\begin{aligned}
\frac{d\Gamma^Z}{dp^2dq^2}(p^2,q^2) &= \frac{g^6}{8\cdot 192\cdot 192\pi^5}\frac{1}{\cos^6\theta_W}\frac{m_Z^2}{m_H^2}|\vec{p}_V(p^2,q^2)|v_pv_q \\
&\times \frac{1}{(p^2-m_Z^2)^2+m_Z^2\Gamma_Z^2}\;\frac{1}{(q^2-m_Z^2)^2+m_Z^2\Gamma_Z^2}\;\frac{1}{16} \\
&\times \left\{L_1^Z(p^2)P_1^{\mu\nu}(p)+3)F_S^2(p^2)L_0^Z(p^2)P_0^{\mu\nu}(p)\right\} \\
&\times \left\{L_1^Z(q^2)P_1^{\mu\nu}(q)+3F_S^2(q^2)L_0^Z(q^2)P_0^{\mu\nu}(q)\right\},
\end{aligned} \tag{38}$$

where we have written the result in terms of the spin-1 and spin-0 projections of the neutral current lepton tensor listed in Appendix B. The spin-1 and spin-0 propagators $P_1^{\mu\nu}$ and $P_0^{\mu\nu}$ are defined in Eq. (4). The velocity-type parameters v_p and v_q are defined by $v_p = 2|\vec{p}_{\ell p}|/\sqrt{p^2} = \sqrt{1-4m_{\ell p}^2/p^2}$ and $v_q = 2|\vec{p}_{\ell q}|/\sqrt{q^2} = \sqrt{1-4m_{\ell q}^2/q^2}$.

In writing down Eq. (38) we have chosen a $p \leftrightarrow q$ symmetric representation. This symmetric form is very useful when one discusses the identical-particle decay $H \to \tau^+\tau^-\tau^+\tau^-$ where two of the four contributing diagrams have the factorizing form of Eq. (38). To achieve the $p \leftrightarrow q$ symmetry one has to add the scalar pieces to the p-side propagators in Eq. (2), i.e. one replaces $P_1^{\alpha\mu}(p)$ by $P_{0\oplus1}^{\alpha\mu}(p)$ etc. The representation (38) is then obtained by expanding e.g. $\int d\Omega_q\, P_{0\oplus1}^{\alpha\mu}(q)\, L_{\mu'}^{(q)}(q)\, P_{0\oplus1}^{\nu\beta}(q)$ along $P_1^{\alpha\beta}$ and $P_0^{\alpha\beta}$.

The contractions of the propagator factors can be calculated to be

$$P_1^{\mu\nu}(p)P_{1\,\mu\nu}(q) \;:=\; \rho_{U+L}(p^2,q^2) \;=\; 2+\frac{(pq)^2}{p^2q^2} = 2+1+\frac{m_H^2|\vec{p}_{Z^*}|^2}{p^2q^2}, \tag{39}$$

$$P_1^{\mu\nu}(p)P_{0\,\mu\nu}(q) \;:=\; \rho_S(p^2,q^2) \;=\; -1+\frac{(pq)^2}{p^2q^2} \;=\; \frac{m_H^2|\vec{p}_{Z^*}|^2}{p^2q^2}, \tag{40}$$

$$P_0^{\mu\nu}(p)P_{0\,\mu\nu}(q) \;:=\; \rho_{SS}(p^2,q^2) \;=\; \frac{(pq)^2}{p^2q^2} = 1+\frac{m_H^2|\vec{p}_{Z^*}|^2}{p^2q^2}. \tag{41}$$

The transverse and longitudinal pieces in Eq. (39) are given by $\rho_U = 2$ and $\rho_L = (pq)^2/p^2q^2$. The scalar–scalar contribution $\rho_{SS} = P_0^{\mu\nu}(p)P_{0\,\mu\nu}(q)$ in Eq. (38) appears multiplied by the product of helicity-flip factors $m_\ell^2/p^2 \cdot m_\ell^2/q^2$ and can be neglected for all practical purposes.

In the present case we take $m_{\ell p} = m_e$ on the p side and $m_{\ell q} = m_\tau$ on the q side such

Γ^Z		Γ_U^Z/Γ^Z	Γ_L^Z/Γ^Z	Γ_S^Z/Γ^Z
$H \to Z(\to e^+e^-) + Z^*(\to \ell^+\ell^-)$				
$(m_\ell = m_\mu)$	$1.008 \times 10^{-7}\,\mathrm{GeV}$	0.4056	0.5940	0.0004
$(m_\ell = m_\tau)$	$0.968 \times 10^{-7}\,\mathrm{GeV}$	0.4062	0.5525	0.0414
$H \to Z^*(\to e^+e^-) + Z^*(\to \ell^+\ell^-)$				
$(m_\ell = m_\mu)$	$2.449 \times 10^{-7}\,\mathrm{GeV}$	0.3879	0.6119	0.0002
$(m_\ell = m_\tau)$	$2.405 \times 10^{-7}\,\mathrm{GeV}$	0.3881	0.5936	0.0183

Table 3: Total and normalized partial decay rates for the four-body decays $H \to Z(\to e^+e^-) + Z^*(\to \ell^+\ell^-)$ (upper part) and $H \to Z^*(\to e^+e^-) + Z^*(\to \ell^+\ell^-)$ (lower part)

that the symmetric appearance of Eq. (38) is lost. In particular, we set $v_p = 1$ and take the $m_\ell \to 0$ limit of the first curly bracket in Eq. (38) replacing it by $(v_\ell^2 + a_\ell^2)P_1^{\mu\nu}(p)$.

In the lower part of Table 3 we present our numerical results for the off-shell – off-shell case. We list the total exclusive decay rate Γ^Z and the averages of the partial decay rates Γ_U^Z/Γ^Z, Γ_L^Z/Γ^Z and Γ_S^Z/Γ^Z for $m_\ell = m_\mu$ (first line) and $m_\ell = m_\tau$ (second line) on the q side ($m_\ell = m_{\ell q}$). For the p side we specify to $m_{\ell p} = m_e$. The off-shell – off-shell rates can be seen to be approximately twice as big as the on-shell – off-shell rates. The reason is that in the off-shell – off-shell case one picks up contributions from the peaking regions on both the p and q side. The helicity fractions remain practically unchanged except for the scalar contribution which is reduced by $\sim 50\,\%$. The reason is that the scalar contribution comes only from the q side whereas the normalizing rate is approximately doubled. Our result agrees with the result $\Gamma^Z = 1.0256 \cdot 10^{-5}\,\mathrm{GeV}$ of Ref. [43] within $1.5\,\%$.

One can undo the smearing in Eq. (38) by the zero-width substitution

$$\frac{1}{(p^2 - m_V^2)^2 + m_V^2\Gamma_V^2} \to \frac{\pi}{m_V\Gamma_V}\delta(p^2 - m_V^2) \tag{42}$$

with $V = Z$. One then obtains

$$\begin{aligned}
\frac{d\Gamma_q^Z}{dq^2}(q^2) &= \frac{g^4}{4\cdot 1536\pi^3}\frac{1}{\cos^4\theta_W}\frac{|\vec{p}_V(p^2,q^2)|v_q}{m_H^2} \\
&\quad\times \frac{B_{Z\ell\ell}}{(q^2-m_Z^2)^2+m_Z^2\Gamma_Z^2}\, m_Z^2\left\{L_1^Z(q^2)\rho_{U+L}(m_Z^2,q^2)+3L_0^Z(q^2)F_S^2(q^2)\rho_S(m_Z^2,q^2)\right\} \\
&= B_{Z\ell\ell}m_Z^2 C^Z(q^2)\left\{L_1^Z(q^2)\rho_{U+L}(m_Z^2,q^2)+3L_0^Z(q^2)F_S^2(q^2)\rho_S(m_Z^2,q^2)\right\}, \qquad (43)
\end{aligned}$$

where $d\Gamma_q^Z/dq^2$ denotes the differential rate into the q–side leptonic mode. As expected, this result coincides with Eq. (35). The result for the (semi-inclusive) three-body decay $H \to Z + Z^*(\to \ell^+\ell^-)$ can be easily obtained from Eq. (43) by summing over all channels, i.e. by skipping the branching ratio factor $B_{Z\ell\ell}$. The result (43) without the factor $B_{Z\ell\ell}$ can be seen to coincide with the result of Ref. [41].

Finally, also the q-side secondary decay process can be considered to be exclusive. Using the decay rate for the decay $Z \to \ell^+\ell^-$ in Eq. (19) for both the p and q sides, from Eq. (38) one obtains

$$\begin{aligned}
\frac{d\Gamma_{pq}^Z}{dp^2dq^2}(p^2,q^2) &= \frac{1}{2}\,\frac{g^2m_Z^2}{8\pi\cos^2\theta_W}\,\frac{|\vec{p}_V(p^2,q^2)|v_pv_q}{m_H^2(v_\ell^2+a_\ell^2)^2} \\
&\quad\times \frac{B_{Z\ell\ell_p}\,m_Z\Gamma_Z}{\pi\left((p^2-m_Z^2)^2+m_Z^2\Gamma_Z^2\right)}\,\frac{B_{Z\ell\ell_q}\,m_Z\Gamma_Z}{\pi\left((q^2-m_Z^2)^2+m_Z^2\Gamma_Z^2\right)}\,\frac{p^2q^2}{m_Z^4} \\
&\quad\times\left\{v_\ell^2(1+2\frac{m_{\ell p}^2}{p^2})P_1^{\mu\nu}(p)+a_\ell^2v_p^2P_1^{\mu\nu}(p)+3a_\ell^2\cdot 2\frac{m_{\ell p}^2}{p^2}F_S^2(p^2)P_0^{\mu\nu}(p)\right\} \\
&\quad\times\left\{v_\ell^2(1+2\frac{m_{\ell q}^2}{q^2})P_{1\,\mu\nu}(q)+a_\ell^2v_q^2P_{1\,\mu\nu}(q)+3a_\ell^2\cdot 2\frac{m_{\ell q}^2}{q^2}F_S^2(q^2)P_{0\,\mu\nu}(q)\right\}. \qquad (44)
\end{aligned}$$

Γ_{pq}^W denotes the rate into the exclusive leptonic modes on the p and q sides, respectively. In the product $B_{Z\ell\ell_p}B_{Z\ell\ell_q}$ there are terms diagonal and nondiagonal in flavour. The nondiagonal terms appear in pairs referring to the same exclusive channel. Thus one has to divide by a factor of two in Eq. (44) as concerns the nondiagonal terms. The diagonal terms appear only once in the product. In the approximation that the interference contributions of the diagonal terms can be neglected, the factor 1/2 correctly counts the number of diagonal terms (see the discussion in Ref. [35]). From the inclusive point of view the

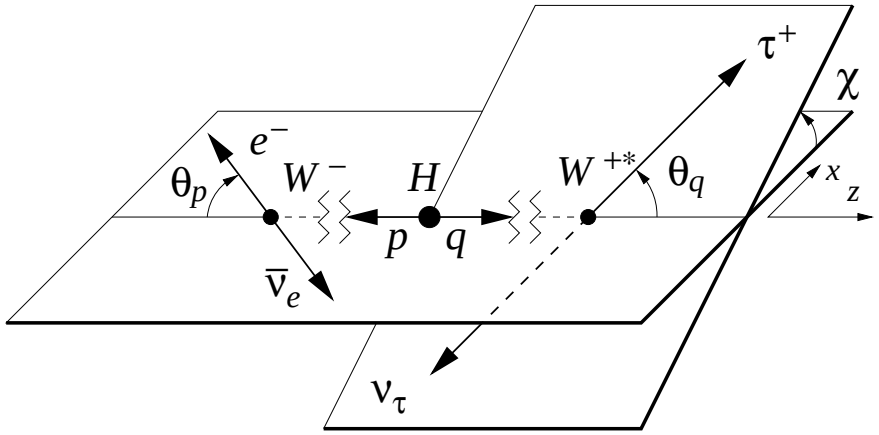


Figure 7: Definition of the momenta p and q, the polar angles θ_p and θ_q, and the azimuthal angle χ in the cascade decay $H \to W^-(\to \ell^-\bar{\nu}_\ell) + W^{+*}(\to \tau^+\nu_\tau)$

factor 1/2 in Eq. (44) appropriately accounts for the identical particle factor of 1/2 in the rate.

It is noteworthy that Eq. (44) cannot be obtained in any gauge without considering the coupling of the off-shell gauge bosons to fermion pairs. If one calculates the rate for $H \to Z^*Z^*$ in the spin-1 Lorenz gauge (also called Landau gauge), the result has to be multiplied by the effective factors p^2/m_Z^2 and q^2/m_Z^2 in order to obtain Eq. (44).

4 The four-body decay $H \to W^-(\to \ell^-\bar{\nu}_\ell) + W^{+*}(\to \tau^+\nu_\tau)$

Even though the yield of the $(H \to \ell\nu\ell\nu)$ mode from Higgs decay is about 40 times larger than the yield of the $(H \to \ell\ell\ell'\ell')$ mode, the identification of the $H \to \ell\nu\ell\nu$ mode is much more difficult experimentally but can nevertheless be done [6]. In this section we write down the three-fold angular decay distribution of the cascade decay $H \to W^-(\to \ell^-\bar{\nu}_\ell) + W^{+*}(\to \tau^+\nu_\tau)$. In the charged-current decays there are no identical-particle effects such that one can also e.g. consider the decay $H \to W^-(\to \tau^-\bar{\nu}_\tau) + W^{+*}(\to \tau^+\nu_\tau)$. As in the neutral-current case the τ mass can be safely neglected on the on-shell side since

the scale is set by the W mass. At the end of this section we shall also discuss off-shell – off-shell decays where the τ mass can no longer be neglected on the p side. A new feature appearing in the charged-current decays is the presence of a scalar–longitudinal interference effect which is parity-conserving but can mimic a parity-violating contribution. One can anticipate without explicit calculation that lepton-mass effects are not as important in the charged-current case since the corresponding helicity-flip contributions are four times weaker than in the neutral-current case. It is for this reason that we do not discuss the charged-current case in as much detail as the neutral-current case.

4.1 Three-fold angular decay distribution for the four-body decay $H \to W^-(\to \ell^-\bar{\nu}_\ell) + W^{+*}(\to \tau^+\nu_\tau)$

Let us first consider the three-fold angular decay distribution of the decay $H \to W^-(\to \ell^-\bar{\nu}_\ell) + W^{+*}(\to \tau^+\nu_\tau)$. The polar angles θ_p and θ_q are defined in the respective lepton pair center-of-mass systems while the azimutal angle χ again describes the relative orientation of the planes as shown in Fig. 7. We use the zero lepton-mass approximation for the on-shell decay $W^- \to \ell^-\bar{\nu}_\ell$ but keep the τ mass finite for the off-shell decay $W^{+*} \to \tau^+\nu_\tau$.

Again we split the angular decay distribution into its helicity-nonflip and helicity-flip part. Accordingly we write

$$W^W(\theta_p, \theta_q, \chi) = W^W_{nf}(\theta_p, \theta_q, \chi) + W^W_{hf}(\theta_p, \theta_q, \chi). \tag{45}$$

The nonflip decay distribution is given by

$$\begin{aligned} W^W_{nf}(\theta_p, \theta_q, \chi) \;=\; & 2p^2 2q^2 v_q \times \\ & \Big\{(\rho_{++} + \rho_{--})\Big[(1+\cos^2\theta_p)(1+\cos^2\theta_q) - 4\cos\theta_p\cos\theta_q\Big] + 4\rho_{00}\sin^2\theta_p\sin^2\theta_q \\ & - 2(\rho_{++} - \rho_{--})(\cos\theta_p - \cos\theta_q)(1 - \cos\theta_p\cos\theta_q) \\ & - 4(\rho_{+0} + \rho_{-0})\sin\theta_p\sin\theta_q(1 - \cos\theta_p\cos\theta_q)\cos\chi + 2\rho_{+-}\sin^2\theta_p\sin^2\theta_q\cos 2\chi \\ & + 4(\rho_{+0} - \rho_{-0})\sin\theta_p\sin\theta_q(\cos\theta_p - \cos\theta_q)\cos\chi\Big\} \end{aligned} \tag{46}$$

($p^2 = m_W^2$). For the flip contribution one obtains

$$\begin{aligned} W_{hf}^W(\theta_p,\theta_q,\chi) \;=\; & \frac{m_\tau^2}{q^2}\cdot 2p^2 2q^2 v_q\Big\{(\rho_{++}+\rho_{--})(1+\cos^2\theta_p)\sin^2\theta_q \\ & + 4\rho_{00}\sin^2\theta_p\cos^2\theta_q - 2(\rho_{++}-\rho_{--})\cos\theta_p\sin^2\theta_q \\ & - 8F_S\rho_{0t}\sin^2\theta_p\cos\theta_q + 4F_S^2\rho_{tt}\sin^2\theta_p - (\rho_{+0}+\rho_{-0})\sin 2\theta_p\sin 2\theta_q\,\cos\chi \\ & + 2(\rho_{+0}-\rho_{-0})\sin\theta_p\sin 2\theta_q\,\cos\chi + 2F_S(\rho_{+t}+\rho_{-t})\sin 2\theta_p\sin\theta_q\,\cos\chi \\ & - 4F_S(\rho_{+t}-\rho_{-t})\sin\theta_p\sin\theta_q\,\cos\chi - 2\rho_{+-}\sin^2\theta_p\sin^2\theta_q\,\cos 2\chi\Big\}, \end{aligned} \tag{47}$$

including the extra minus sign for the spin-1 – spin-0 interference contributions linear in F_S. We have used the velocity-type parameter $v_q = 2|\vec{p}_{\ell q}|/\sqrt{q^2} = 1 - m_{\ell q}^2/q^2$.

In Eqs. (46) and (47) we have also included the contributions from the parity-violating terms proportional to $(\rho_{++}-\rho_{--})$, $(\rho_{+0}-\rho_{-0})$ and $(\rho_{+t}-\rho_{-t})$. These coefficient functions are not populated by the parity-conserving SM (HVV) coupling. In Appendix A we briefly discuss the contribution of a parity-violating non-SM coupling proportional to $\epsilon^{\mu\nu\rho\sigma}p_\rho q_\sigma$ which would populate the $(\rho_{++}-\rho_{--})$, $(\rho_{+0}-\rho_{-0})$ and $(\rho_{+t}-\rho_{-t})$ coefficient functions [17, 18, 19].

Again we write the result in terms of the Legendre polynomials $P_1(\cos\theta) = \cos\theta$ and $P_2(\cos\theta) = \frac{1}{2}(3\cos^2\theta - 1)$,

$$(2p^2 2q^2)^{-1} W^W(\theta_p,\theta_q,\chi) = \frac{16 v_q}{9}\sum_{i=0}^{10}\mathcal{F}_i^W h_i(\theta_p,\theta_q,\chi) = \frac{16 v_q}{9}\sum_{i=0}^{10}(f_i^W + \varepsilon g_i^W) h_i(\theta_p,\theta_q,\chi). \tag{48}$$

The coefficient functions f_i^W and g_i^W can be found in Table 4 where we have now dropped the non-SM contributions proportional to $(\rho_{++}-\rho_{--})$, $(\rho_{+0}-\rho_{-0})$ and $(\rho_{+t}-\rho_{-t})$. It is noteworthy that three new angular structures proportional to $\cos\theta_q$ ($i = 8, 9$) and $\sin\theta_q$ ($i = 10$) are generated by a helicity-flip contribution. The first of these contributions ($i = 8$) give rise to a nonvanishing forward-backward asymmetry in the $\cos\theta_q$ distribution as discussed later on.

i	f_i^W	g_i^W	$h_i(\theta_p, \theta_q, \chi)$
0	ρ_{U+L}	$\frac{1}{2}\rho_{U+L} + \frac{3}{2}F_S^2\rho_S$	1
1	$\frac{1}{2}(\rho_U - 2\rho_L)$	$-\frac{1}{2}(\rho_U - 2\rho_L)$	$P_2(\cos\theta_q)$
2	$\frac{1}{2}(\rho_U - 2\rho_L)$	$\frac{1}{4}(\rho_U - 2\rho_L) - \frac{3}{2}F_S^2\rho_S$	$P_2(\cos\theta_p)$
3	$\frac{1}{4}(\rho_U + 4\rho_L)$	$-\frac{1}{4}(\rho_U + 4\rho_L)$	$P_2(\cos\theta_p)P_2(\cos\theta_q)$
4	$-\frac{9}{4}\rho_U$	0	$\cos\theta_p \cos\theta_q$
5	$-\frac{9}{4}(\rho_{+0} + \rho_{-0})$	0	$\sin\theta_p \sin\theta_q \cos\chi$
6	$\frac{9}{16}(\rho_{+0} + \rho_{-0})$	$-\frac{9}{16}(\rho_{+0} + \rho_{-0})$	$\sin 2\theta_p \sin 2\theta_q \cos\chi$
7	$\frac{9}{8}\rho_{+-}$	$-\frac{9}{8}\rho_{+-}$	$\sin^2\theta_p \sin^2\theta_q \cos 2\chi$
8	0	$-3F_S\,\rho_{0t}$	$\cos\theta_q$
9	0	$3F_S\,\rho_{0t}$	$P_2(\cos\theta_p)\cos\theta_q$
10	0	$\frac{9}{8}\,F_S(\rho_{+t} + \rho_{-t})$	$\sin 2\theta_p \sin\theta_q \cos\chi$

Table 4: Coefficient functions appearing in the three-fold angular decay distribution of the decay $H \to W^-(\to \ell^-\bar{\nu}_\ell) + W^{+*}(\to \tau^+\nu_\tau)$.

We define a normalized decay distribution

$$\widetilde{W}^W(\theta_p, \theta_q, \chi) = \frac{W^W(\theta_p, \theta_q, \chi)}{\int W^W(\theta_p', \theta_q', \chi')d\cos\theta_p'\, d\cos\theta_q'\, d\chi'} = \frac{1}{8\pi}\Big(1 + \sum_{i=1}^{9} \widetilde{\mathcal{F}}_i^W h_i(\theta_p, \theta_q, \chi)\Big), \quad (49)$$

where $\widetilde{\mathcal{F}}_i^W = \mathcal{F}_i^W/\mathcal{F}_0^W$ (and $\tilde{f}_i^W = f_i^W/\mathcal{F}_0^W$, $\tilde{g}_i^W = g_i^W/\mathcal{F}_0^W$) and where

$$\mathcal{F}_0^W = f_0^W + \varepsilon g_0^W = \rho_{U+L} + \tfrac{1}{2}\varepsilon(\rho_{U+L} + 3F_S^2\rho_S). \quad (50)$$

The differential decay rate distribution is given by

$$\frac{d\Gamma^W}{dq^2\, d\cos\theta_p\, d\cos\theta_q\, d\chi} = B_{W\ell\nu}\frac{C^W(q^2)}{8\pi} \times \frac{9}{16v_q} W^W(q^2, \theta_p, \theta_q, \chi), \quad (51)$$

where

$$C^W(q^2) = \frac{g^4 v_q}{1536\pi^3} \frac{|\vec{p}_V(m_W^2, q^2)| v_q}{m_H^2} \frac{1}{(q^2 - m_W^2)^2 + m_W^2 \Gamma_W^2} \tag{52}$$

(note the additional factor v_q in the numerator) and $B_{W\ell\nu} = \Gamma_{W\ell\nu}/\Gamma_W$. The decay rate for $W \to \ell\nu$ ($m_\ell = 0$) is given by

$$\Gamma_{W\ell\nu} = \Gamma(W \to \ell\nu) = \frac{g^2}{48\pi} m_W. \tag{53}$$

Partial differential rates are defined according to

$$\frac{d\,\Gamma_i^W}{dq^2} = 2p^2\, 2q^2 B_{W\ell\nu} C^W(q^2) \mathcal{F}_i^W(q^2). \tag{54}$$

The average values $\langle \widetilde{\mathcal{F}}_i^W \rangle$ of the coefficient functions is given by

$$\langle \widetilde{\mathcal{F}}_i^W \rangle = \frac{\int dq^2 2p^2 2q^2 B_{W\ell\nu} C^W(q^2) \mathcal{F}_i^W(q^2)}{\int dq^2 2p^2 2q^2 B_{W\ell\nu} C^W(q^2) \mathcal{F}_0^W(q^2)} = \frac{\Gamma_i^W}{\Gamma^W}, \tag{55}$$

where the integration over q^2 runs from $4m_\ell^2$ to $(m_H - m_W)^2$.

In Table 5 we present numerical results for the normalized coefficient functions $\widetilde{\mathcal{F}}_i^W(q^2)$ and their averages. In columns 2 and 3 we list the values of $\widetilde{\mathcal{F}}_i^W(q^2)$ for $q^2 = 50\,\mathrm{GeV}^2$ with zero and nonzero lepton masses. Lepton-mass effects amount to -16% for the functions $\widetilde{\mathcal{F}}_{1,3,6,7}^W$, -11.8% for the functions $\widetilde{\mathcal{F}}_{4,5}^W$, and only $+0.4\%$ for the function $\widetilde{\mathcal{F}}_2^W$. The normalized coefficient functions $\widetilde{\mathcal{F}}_{8,9,10}^W$ are zero for zero lepton masses. For $m_\ell = m_\tau$ the coefficient functions $\widetilde{\mathcal{F}}_{8,9}^W$ become quite large at 16.1%. Again, lepton-mass effects would be even larger for smaller values of q^2. Compared to the $H \to ZZ^*$ case, lepton mass effects are smaller by approximately a factor of 1/2.

In columns 4 and 5 of Table 5 we also present average values $\langle \widetilde{\mathcal{F}}_i^W \rangle$ of the coefficient functions again for zero and nonzero lepton masses where the average is taken with regard to q^2. On average lepton mass effects can be seen to be quite small.

i	$\widetilde{\mathcal{F}}_i^W\ (m_\ell = 0)$	$\widetilde{\mathcal{F}}_i^W\ (m_\ell = m_\tau)$	$\langle\widetilde{\mathcal{F}}_i^W\rangle\ (m_\ell = 0)$	$\langle\widetilde{\mathcal{F}}_i^W\rangle\ (m_\ell = m_\tau)$
1	-0.9549	-0.7983	-0.3965	-0.3817
2	-0.9549	-0.9585	-0.3965	-0.3985
3	$+0.9775$	$+0.8172$	$+0.6983$	$+0.6809$
4	-0.6759	-0.0603	-0.9052	-0.9006
5	-0.5431	-0.4847	-1.4306	-1.4205
6	$+0.1358$	$+0.1135$	$+0.3576$	$+0.3533$
7	$+0.0169$	$+0.0141$	$+0.2263$	$+0.2244$
8	-0.0000	-0.1614	-0.0000	-0.0176
9	$+0.0000$	$+0.1614$	$+0.0000$	$+0.0176$
10	$+0.0000$	$+0.0015$	$+0.0000$	$+0.0029$

Table 5: Numerical results for the normalized coefficient functions $\widetilde{\mathcal{F}}_i^W(q^2)$ at $q^2 = 50\,\mathrm{GeV}^2$ and the average of $\widetilde{\mathcal{F}}_i^W(q^2)$ over $q^2 \in [m_\ell^2, (m_H - m_W)^2]$

4.2 Forward-backward asymmetry of the τ^+ lepton

Let us take a closer look at the $\cos\theta_q$ distribution determined by the coefficient functions $\widetilde{\mathcal{F}}_1^W$ and $\widetilde{\mathcal{F}}_8^W$. The normalized $\cos\theta_q$ distribution is given by (see Table 4)

$$\widetilde{W}^W(q^2,\theta_q) = \frac{1}{2}\left(1 + \widetilde{\mathcal{F}}_1^W P_2(\cos\theta_q) + \widetilde{\mathcal{F}}_8^W \cos\theta_q\right). \tag{56}$$

Contrary to the $H \to ZZ^*$ case one now has a contribution linear in $\cos\theta_q$ which implies a nonvanishing forward-backward asymmetry. It is interesting to note that the source of this parity-odd term in Eq. (57) results from a parity-conserving interaction. Consider the J^P content of the currents coupling to the W^*: $V^\mu(1^-,0^+)$ and $A^\mu(1^+,0^-)$. The scalar–longitudinal interference contribution leading to a nonvanishing forward-backward asymmetry can be seen to result from the parity-conserving interference of the products of currents $V(0^+)V(1^-)$, $A(0^-)A(1^+)$. We mention that a parity-violating (HW^+W^-) coupling as discussed in Appendix A would also give rise to a nonvanishing forward-backward asymmetry proportional to $(\rho_{++} - \rho_{--})$ (see Eq. (46)).

In Fig. 8 we display the normalized $\cos\theta_q$ distribution for a fixed value of $q^2 = 50\,\mathrm{GeV}^2$. Since $\rho_U \ll \rho_L$ for $q^2 = 50$ GeV^2, the governing feature of the distribution is described by a downward open parabola. The convexity parameter is proportional to $(1-\varepsilon)$, leading to a smaller convexity for the $m_\ell = m_\tau$ distribution as can be seen in Fig. 8. There is a pronounced forward-backward asymmetry in the τ mode. According to Eq. (56) the forward-backward asymmetry of the $\cos\theta_q$ distribution is given by

$$A_{FB}(q^2) = \frac{\Gamma_F - \Gamma_B}{\Gamma_F + \Gamma_B} = \frac{1}{2}\widetilde{\mathcal{F}}_8^W(q^2) = \frac{m_\ell^2}{q^2} \times \frac{-3F_S(q^2)\rho_{0t}(q^2)}{2\mathcal{F}_0^W(q^2)}. \tag{57}$$

Since ρ_{0t} and F_S are positive, the forward-backward asymmetry A_{FB} is negative as also shows up in Fig. 8. In fact, one calculates

$$A_{FB}(q^2 = 50\,\mathrm{GeV}^2) = -0.081. \tag{58}$$

For smaller q^2 values the forward-backward asymmetry becomes even more pronounced. In the last column of Table 6 we list the average value of A_{FB} which is given by $\langle A_{FB}\rangle =$

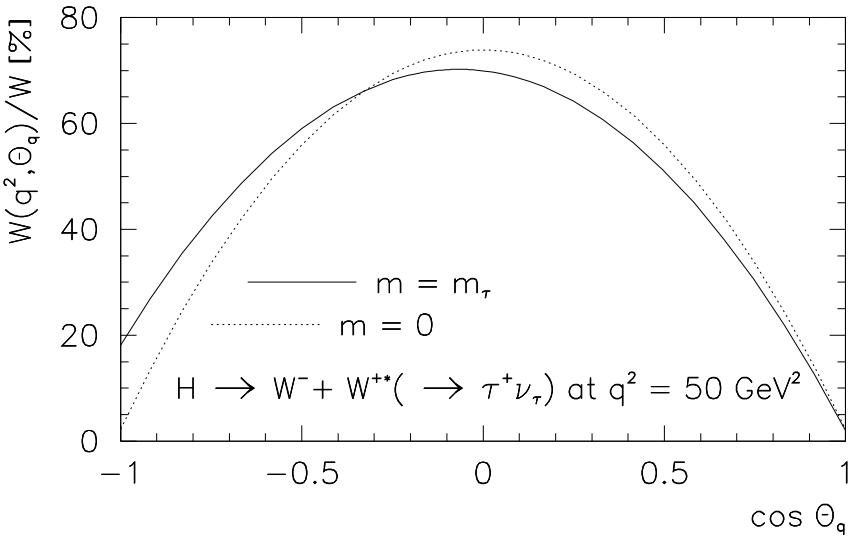


Figure 8: $\cos\theta_q$ dependence of the normalized decay distribution $\widetilde{W}^W(q^2,\theta_q)$ for $q^2 = 50\,\mathrm{GeV}^2$ for $m_\ell = 0$ (dotted line) and $m_\ell = m_\tau$ (solid line)

$\frac{1}{2}\langle\widetilde{\mathcal{F}}_8^W\rangle$. On average, the forward-backward asymmetry is much smaller than for $q^2 = 50\,\mathrm{GeV}^2$.

4.3 The polarization of the off-shell W^{+*}

Let us rewrite the single-angle $\cos\theta_q$ distribution in Eq. (56) in terms of the transverse, longitudinal, scalar and the scalar–longitudinal interference contributions. One has

$$\begin{aligned}\frac{d\Gamma^W}{dq^2 d\cos\theta_q} &= 2p^2 2q^2 B_{W\ell\nu} C^W(q^2)\Big\{\frac{3}{8}(1+\cos^2\theta_q)\rho_U + \frac{3}{4}\sin^2\theta_q\rho_L \\ &+\frac{m_\ell^2}{2q^2}\Big[\frac{3}{4}\sin^2\theta_q\rho_U + \frac{3}{2}\cos^2\theta_q\rho_L - 3F_S(q^2)\cos\theta_q\rho_{t0} + \frac{3}{2}F_S^2(q^2)\rho_S\Big]\Big\}. \qquad (59)\end{aligned}$$

Integrating the differential rate (34) with respect to $\cos\theta_q$, one obtains

$$\frac{d\Gamma^W}{dq^2} = 2p^2\,2q^2\,B_{W\ell\nu}C^W(q^2)\left\{(\rho_U+\rho_L) + \frac{m_\ell^2}{2q^2}\Big[(\rho_U+\rho_L) + 3F_S^2(q^2)\rho_S\Big]\right\}. \qquad (60)$$

Partial decay rates are accordingly defined by

$$\frac{d\Gamma^W_{U,L}}{dq^2} = 2p^2\,2q^2\,B_{W\ell\nu}C^W(q^2)\left(1+\frac{m_\ell^2}{2q^2}\right)\rho_{U,L}\,,$$

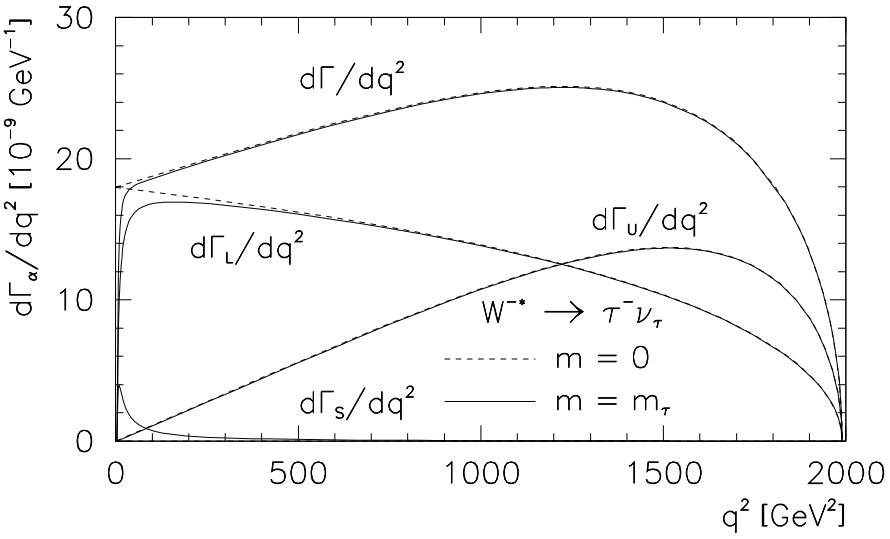


Figure 9: Differential rates $d\Gamma_\alpha^W/dq^2$ (indices $\alpha = U, L, S$ and vanishing index for $\alpha = U+L$) for the decay $H \to W^-(\to e^-\bar{\nu}_e) + W^{+*}(\to \ell^+\nu_\ell)$ with $m_\ell = 0$ and $m_\ell = m_\tau$

$$\frac{d\Gamma_S^W}{dq^2} \;=\; 2p^2\, 2q^2\, B_{W\ell\nu} C^W(q^2) \frac{3m_\ell^2}{2q^2}\, F_S^2(q^2)\rho_S. \tag{61}$$

In Fig. 9 we display the q^2 dependence of the partial decay rates. Lepton-mass effects show up mainly for lower q^2 values between threshold and approximately $150\,\mathrm{GeV}^2$. For example, at $q^2 = 50\,\mathrm{GeV}^2$ the helicity fractions of the W^{+*} change according to

$$\widetilde{U} : \widetilde{L} : \widetilde{S} = 0.030 : 0.970 : 0 \qquad \to \qquad \widetilde{U} : \widetilde{L} : \widetilde{S} = 0.028 : 0.893 : 0.079 \tag{62}$$

when going from the e, μ modes to the τ mode. The picture is similar to the $H \to ZZ^*$ case. However, lepton-mass effects are less pronounced in the $H \to WW^*$ case.

In the upper part of Table 6 we list the total rate and the mean values of the transverse, longitudinal and scalar partial rates for the mass-zero modes and the τ mode where the mean is taken with regard to q^2. In this case, lepton-mass effects reduce the total rate by 0.76 %. The rate reduction is largest for the longitudinal rate where the rate reduction amounts to 2.1 %. On average, the rate reduction for $\langle\, \Gamma_L \rangle = \Gamma_L/\Gamma$ is still a considerable 1.3 % while the average of the transverse rate is practically unchanged. As in the $W \to ZZ^*$

case, the loss of longitudinal rate is mainly compensated for by the appearance of the scalar rate. Our result agrees with the result $\Gamma^W = 2.4135 \cdot 10^{-7}\,\mathrm{GeV}$ of Ref. [43] within 1.6 %.

4.4 Off-shell – off-shell decays $H \to W^{-*}(\to \ell^- \bar{\nu}_\ell) + W^{+*}(\to \tau^+ \nu_\tau)$

Again, we conclude the section by considering the case where both W bosons are off-shell. Using again the narrow-width approximation (42) for $V = W$ also on the p side, the exclusive off-shell – off-shell rate is obtained from the double integral

$$\Gamma^W_{pq} = \int_{m^2_{\ell p}}^{m^2_H} dp^2 \frac{B_{W\ell\nu p}\, m_W \Gamma_W}{\pi((p^2 - m_W^2)^2 + m_W^2\Gamma_W^2)} \int_{m^2_{\ell q}}^{(m_H - \sqrt{p^2})^2} dq^2 \frac{B_{W\ell\nu q}\, m_W \Gamma_W}{\pi((q^2 - m_W^2)^2 + m_W^2\Gamma_W^2)} \Gamma_0^W\,, \tag{63}$$

where Γ^W_{pq} denotes the rate into the exclusive leptonic modes on the p and q sides. The total inclusive mode is obtained by summing over all exclusive modes including the quark–antiquark modes, i.e. by setting $B_{W\ell\nu p} = B_{W\ell\nu q} = 1$. The rate function Γ_0^W in Eq. (63) reads

$$\begin{aligned} \Gamma_0^W &= \frac{g^2}{8\pi} |\vec{p}_V(p^2, q^2)| \frac{1}{m_W^2 m_H^2} \frac{v_p v_q}{64} \Big\{ L_1^W(p^2) P_1^{\mu\nu}(p) + 3F_S^2(p^2) L_0^W(p^2) P_0^{\mu\nu}(p) \Big\} \\ &\quad \times \Big\{ L_1^W(q^2) P_1^{\mu\nu}(q) + 3F_S^2(q^2) L_0^W(q^2) P_0^{\mu\nu}(q) \Big\}, \end{aligned} \tag{64}$$

where $v_p = 1 - m^2_{\ell p}/p^2$ and $v_q = 1 - m^2_{\ell q}/q^2$. L_1^W and L_0^W are the spin-1 and spin-0 projections of the charged current lepton tensors listed in Appendix C. When the lepton masses are taken to be zero, the rate function (64) simplifies to

$$\Gamma_0^W(m_\ell = 0) = \frac{g^2}{8\pi} |\vec{p}_W| \frac{p^2 q^2}{m_W^2 m_H^2}\, \rho_{U+L} \tag{65}$$

which agrees with the results in Refs. [42, 44].

In Table 6 we have listed our numerical results for the off-shell – off-shell rates and the averages of the polarization of the gauge bosons. The off-shell – off-shell rates approximately amount to two times the off-shell – on-shell rates. The reason is again that one picks up contributions from the peaking regions both on the p side and on the q side. Put

	Γ^W	Γ_U^W/Γ^W	Γ_L^W/Γ^W	Γ_S^W/Γ^W	$\langle A_{FB}\rangle$
$H \to W^-(\to e^-\bar{\nu}_e) + W^{+*}(\to \ell^+\nu_\ell)$					
$(m_\ell = m_\mu)$	$4.754 \times 10^{-6}\,\mathrm{GeV}$	0.4023	0.5976	0.0001	-5×10^{-5}
$(m_\ell = m_\tau)$	$4.718 \times 10^{-6}\,\mathrm{GeV}$	0.4033	0.5894	0.0073	-0.0059
$H \to W^{-*}(\to e^-\bar{\nu}_e) + W^{+*}(\to \ell^+\nu_\ell)$					
$(m_\ell = m_\mu)$	$1.009 \times 10^{-5}\,\mathrm{GeV}$	0.3952	0.6048	3×10^{-5}	-2×10^{-5}
$(m_\ell = m_\tau)$	$1.005 \times 10^{-5}\,\mathrm{GeV}$	0.3956	0.6009	0.0035	-0.0029
$H \to W^{-*}(\to \ell^-\bar{\nu}_\ell) + W^{+*}(\to \ell^+\nu_\ell)$					
$(m_\ell = m_\mu)$	$1.009 \times 10^{-5}\,\mathrm{GeV}$	0.3952	0.6048	6×10^{-5}	-6×10^{-5}
$(m_\ell = m_\tau)$	$1.001 \times 10^{-5}\,\mathrm{GeV}$	0.3960	0.5970	0.0070	-0.0076

Table 6: Total and normalized partial decay rates and the average value of the forward-backward symmetry for the four-body decays $H \to W^-(\to e^-\bar{\nu}_e) + W^{+*}(\to \ell^+\nu_\ell)$ (first part), $H \to W^{-*}(\to e^-\bar{\nu}_e)+W^{+*}(\to \ell^+\nu_\ell)$ (second part), and $H \to W^{-*}(\to \ell^-\bar{\nu}_\ell)+W^{+*}(\to \ell^+\nu_\ell)$ (third part)

in a different language the off-shell – off-shell rate (63) corresponds to the sum of the two off-shell – on-shell rates $H \to W^-W^{+*}$ and $H \to W^{-*}W^+$. The polarizations listed in Table 6 are thus an average of the respective polarizations on the p side and the q side. This also explains the fact that the scalar polarization is only one-half of the on-shell – off-shell value since it is contributed to only by the q side $H \to W^-W^{+*}$ channel. This is no longer true for the $H \to W^{-*}(\to \tau^-\bar{\nu}_\tau) + W^{+*}(\to \tau^+\nu_\tau)$ mode where the scalar rate obtains contributions from both the p side and the q side.

The off-shell – off-shell rates slightly exceed twice the off-shell – on-shell rates which provides a measure of the quality of taking the zero-width approximation on the on-shell sides. Compared to the rates for $H \to Z^*Z^*$ listed in Table 3, lepton-mass effects can be

seen to be more than five times smaller in the $H \to W^{-*}W^{+*}$ case.

5 Summary and conclusions

We have discussed lepton-mass effects in the rate and the angular decay distributions in the four-body decays $H \to Z(\to \ell^+\ell^-) + Z^*(\to \tau^+\tau^-)$ and $H \to W^-(\to \ell^-\bar{\nu}_\ell) + W^{+*}(\to \tau^+\nu_\tau)$ where the gauge bosons Z and W^- are on their mass shell. Lepton-mass effects are larger for the $H \to ZZ^*$ mode where we find a reduction of 3.97 % in the τ rate relative to the e, μ rates. In the $H \to WW^*$ case the rate reduction of the total rate is smaller. In this mode we find a rate reduction of 0.76 % relative to the zero mass case. Differentially, the rate reduction through lepton-mass effects is significantly larger at the lower end of the q^2 spectrum in both cases. For both modes we find a significant reduction of the longitudinal rate through lepton-mass effects in the lower q^2 region from threshold to $\sim 200\,\mathrm{GeV}^2$. In this region the transverse–longitudinal composition of the off-shell gauge bosons is considerably changed. The reduction of the longitudinal rate in this region is partly compensated for by a significant scalar contribution. In the charged-current case one finds a nonvanishing forward-backward asymmetry in the $\cos\theta_q$ distribution through lepton-mass induced scalar–longitudinal interference effects. The forward-backward asymmetry can become quite large in the low-q^2 region.

We have also discussed the case when both gauge-bosons go off-shell. Double smearing with the appropriate Breit–Wigner functions increases the overall rate. Lepton-mass effects become weaker in the double smearing process.

We have employed helicity methods in our analysis which has allowed us to present our analytical results for angular decay distributions and partial rates in compact form. In particular, the inclusion of lepton-mass effects in the helicity formalism is straightforward.

Experimentally it will not be so simple to identify the τ modes in the four-lepton decays of the Higgs. In this context we mention that the detection efficiency for τ leptons

in their hadronic decay channels at the LHC is being continuously improved (see Refs. [45, 46, 47]). Nevertheless, an accurate Monte Carlo event generator for decays involving the τ leptons should include lepton-mass effects for which we have supplied the appropriate matrix elements in this paper. This would e.g. be relevant for modelling $Z \to \tau\tau$ processes as background for the search for the decay $H \to \tau^+\tau^-$ [48, 49, 50].

Acknowledgments

This work was supported by the Estonian Research Council under Grant No. IUT2-27. J.G.K. would like to thank A. Denner, B. Jäger, M. Rauch, H. Spiesberger, B. Stech and J. Wang for useful discussions. S.G. acknowledges the support by the Mainz Institute of Theoretical Physics (MITP).

A Helicity amplitudes for $H \to VV^*$

The helicity amplitudes $H_{\lambda_V \lambda_{V^*}}$ for the transition $H \to VV^*$ are defined by

$$H_{mn} = \bar{\varepsilon}^{*\,\alpha}(\lambda_V, p) H_{\alpha\alpha'} \varepsilon^{*\,\alpha'}(\lambda_{V^*}, q), \tag{A1}$$

where $\bar{\varepsilon}^{*\,\alpha}(\lambda_V, p)$ and $\varepsilon^{*\,\alpha'}(\lambda_{V^*}, q)$ are the respective polarization four-vectors on the p side (on-shell side) and on the q side (off-shell side). We shall evaluate the helicity amplitudes in the Higgs rest frame with the z direction defined by the direction of the off-shell V^* boson. One therefore has to rotate the polarization four-vectors on the p side by 180° which we indicate by the "bar" symbol.

The respective polarization four-vectors in the Higgs rest frame are given by

$$\begin{aligned}
\text{on-shell side} \quad : \qquad & \bar{\varepsilon}^{\alpha}(\pm, p) = \frac{1}{\sqrt{2}}(0; \pm 1, -i, 0) \qquad \bar{\varepsilon}^{\alpha}(0, p) = \frac{1}{m_V}(|\vec{p}_V|; 0, 0, -p_0) \\
\text{off-shell side} \quad : \qquad & \varepsilon^{\mu}(\pm, q) = \frac{1}{\sqrt{2}}(0; \mp 1, -i, 0) \qquad \varepsilon^{\mu}(0, q) = \frac{1}{\sqrt{q^2}}(|\vec{p}_V|; 0, 0, q_0) \\
& \varepsilon^{\mu}(t, q) = \frac{1}{\sqrt{q^2}}(q_0; 0, 0, |\vec{p}_V|)
\end{aligned}$$

where $p_0 = (m_H^2 + p^2 - q^2)/(2m_H)$, $q_0 = (m_H^2 + q^2 - p^2)/(2m_H)$ and

$$|\vec{p}_V| = \frac{1}{2m_H}\lambda^{1/2}(m_H^2, p^2, q^2) = \frac{\sqrt{(pq)^2 - p^2q^2}}{m_H} \tag{A2}$$

such that $p^\mu = (p_0; 0, 0, -|\vec{p}_V|)$, $q^\mu = (q_0; 0, 0, |\vec{p}_V|)$. It is convenient to avail of the covariant representations of the longitudinal and scalar polarization four-vectors. They read

$$\begin{aligned}
&\text{on-shell side}: \quad \bar{\varepsilon}^\mu(0) = \frac{1}{\sqrt{p^2}\sqrt{(pq)^2 - p^2q^2}}\Big((pq)p^\mu - p^2q^\mu\Big) \qquad \bar{\varepsilon}^\mu(t) = \frac{p^\mu}{\sqrt{p^2}} \\
&\text{off-shell side}: \quad \varepsilon^\mu(0) = \frac{1}{\sqrt{q^2}\sqrt{(pq)^2 - p^2q^2}}\Big((pq)q^\mu - q^2p^\mu\Big) \qquad \varepsilon^\mu(t) = \frac{q^\mu}{\sqrt{q^2}}
\end{aligned} \tag{A3}$$

The helicity amplitudes can then be calculated to be

$$H_{++} = H_{--} = 1, \qquad H_{00} = H_{tt} = \frac{pq}{\sqrt{p^2}\sqrt{q^2}}, \qquad H_{0t} = H_{t0} = \frac{\sqrt{(pq)^2 - p^2q^2}}{\sqrt{p^2}\sqrt{q^2}} = \frac{m_H|\vec{p}_V|}{\sqrt{p^2}\sqrt{q^2}}. \tag{A4}$$

The coefficient functions $\mathcal{F}_i^{Z,W}$ are written in terms of bilinear forms of the helicity amplitudes for which we choose the following abbreviations

$$\begin{aligned}
\rho_{00} &= |H_{00}|^2, \qquad \rho_{\pm\pm} = |H_{\pm\pm}|^2, \qquad \rho_{tt} = \mathrm{Re}\, H_{0t}H_{0t}^*, \\
\rho_{\pm 0} &= \mathrm{Re}\, H_{\pm\pm}H_{00}^*, \qquad \rho_{\pm\mp} = \mathrm{Re}\, H_{\pm\pm}H_{\mp\mp}^*, \\
\rho_{\pm t} &= \mathrm{Re}\, H_{\pm\pm}H_{0t}^*, \qquad \rho_{t\pm} = \mathrm{Re}\, H_{0t}H_{\pm\pm}^*, \\
\rho_{0t} &= \mathrm{Re}\, H_{00}H_{0t}^*, \qquad \rho_{t0} = \mathrm{Re}\, H_{t0}H_{00}^*.
\end{aligned} \tag{A5}$$

We sometimes refer to these bilinear forms as the double spin-density matrix elements of the gauge boson pair since the bilinear forms describe the entangled polarizations components of the gauge boson pair. The SM values of the double density matrix $\rho_{mm'}$ are given by

$$\begin{aligned}
\rho_{++} = \rho_{--} &= 1, \qquad \rho_{\pm\mp} = 1, \qquad \rho_{00} = \frac{(pq)^2}{p^2q^2} = \Big(1 + \frac{m_H^2}{q^2m_V^2}|\vec{p}_V|^2\Big), \\
\rho_{0t} = \rho_{t0} &= \frac{pq\sqrt{(pq)^2 - p^2q^2}}{p^2q^2} = \frac{m_H|\vec{p}_V|}{2m_V^2q^2}\left(m_H^2 - m_V^2 - q^2\right), \\
\rho_{tt} &= \frac{(pq)^2 - p^2q^2}{p^2q^2} = \frac{m_H^2}{q^2m_V^2}|\vec{p}_V|^2.
\end{aligned} \tag{A6}$$

One notes the following SM relations

$$\rho_{tt} = \rho_{00} - 1, \qquad \rho_{0t} = \sqrt{\rho_{00}\rho_{tt}}, \qquad \rho_{\pm 0} = \rho_{\pm t} = \sqrt{\rho_{00}}. \tag{A7}$$

At maximal recoil where q^2 and/or p^2 tend to zero, the dominant double spin-density matrix elements are $\rho_{00} = \rho_{0t} = \rho_{t0} = \rho_{tt}$. At minimal recoil $q^2 = (m_H - m_V)^2$ where $|\vec{p}_V| \to 0$, the dominant contributions are $\rho_{++} = \rho_{--} = \rho_{00}$ while ρ_{0t} and ρ_{tt} tend to zero.

Some authors prefer to use Cartesian components for the transition matrix elements [18] instead of the helicity components used by us. The relation between the two representations is given by

$$A_\parallel \;=\; \frac{1}{\sqrt{2}}(H_{++} + H_{--}), \qquad A_\perp \;=\; \frac{1}{\sqrt{2}}(H_{++} - H_{--}), \qquad A_0 \;=\; H_{00}. \tag{A8}$$

We see no particular advantages to write the angular coefficient functions in terms of their Cartesian components.

Battacherjee *et al.* considered two additional non-SM (HVV) coupling structures [18]. They write down the effective coupling structure

$$V^{\mu\nu} = a g^{\mu\nu} + b(q^\mu p^\nu - (pq) g^{\mu\nu}) + ic\epsilon^{\mu\nu\rho\sigma} p_\rho q_\sigma. \tag{A9}$$

The helicity components are then given by

$$H_{00} = a\frac{pq}{\sqrt{p^2}\sqrt{q^2}} - b\sqrt{p^2}\sqrt{q^2}, \qquad H_{\pm\pm} = a \mp c\sqrt{(pq)^2 - p^2 q^2}. \tag{A10}$$

There are no contributions of the new coupling structures to H_{0t}. It is clear that one now has a contribution to the difference $(H_{++} - H_{--})$ resulting from the parity-violating term proportional to $\epsilon^{\mu\nu\rho\sigma} p_\rho q_\sigma$.

B Helicity representation of the neutral-current lepton tensor

We calculate the helicity representation of the neutral-current lepton tensor on the off-shell q side. The corresponding expressions for the on-shell p side can be obtained by setting

the lepton mass to zero and replacing $q \to p$. We work in the center-of-mass system of the lepton pair with the z direction defined by ℓ^+ which we refer to as the helicity system. The kinematics in the helicity system is given by

$$\begin{aligned} q^\alpha &= \sqrt{q^2}\,(1;0,0,0) \qquad \ell^{\pm\alpha} = \tfrac{1}{2}\sqrt{q^2}(1;0,0,\pm v_q) \\ \varepsilon^\mu(0) &= (0;0,0,1) \qquad \varepsilon^\mu(\pm) = \frac{1}{\sqrt{2}}(0;\mp 1,-i,0) \qquad \varepsilon^\mu(t) = (1;0,0,0) \end{aligned} \tag{B1}$$

where $v_q^2 = 1 - 4m_q^2/q^2 = 1 - 4\varepsilon$. The covariant forms of the lepton tensors read

$$\begin{aligned} L^{VV}_{\mu\nu} &= \mathrm{Tr}\left(\gamma_\mu(\ell\!\!\!/^+ - m_q)\gamma_\nu(\ell\!\!\!/^- + m_q)\right) = 4\left(\ell^+_\mu\ell^-_\nu + \ell^+_\nu\ell^-_\mu - \tfrac{1}{2}q^2 g_{\mu\nu}\right), \\ L^{AA}_{\mu\nu} &= \mathrm{Tr}\left(\gamma_\mu\gamma_5(\ell\!\!\!/^+ - m_q)\gamma_\nu\gamma_5(\ell\!\!\!/^- + m_q)\right) = 4\left(\ell^+_\mu\ell^-_\nu + \ell^+_\nu\ell^-_\mu - \tfrac{1}{2}(q^2 - 4m_q^2) g_{\mu\nu}\right), \\ L^{VA}_{\mu\nu} &= L^{AV}_{\mu\nu} = \mathrm{Tr}\left(\gamma_\mu(\ell\!\!\!/^+ - m_q)\gamma_\nu\gamma_5(\ell\!\!\!/^- + m_q)\right) = -4i\epsilon_{\mu\nu\rho\sigma}q^\rho\ell^{+\sigma}. \end{aligned} \tag{B2}$$

The total neutral current lepton tensor is composed according to

$$L_{\mu\nu} = v_\ell^2 L^{VV}_{\mu\nu} - 2v_\ell a_\ell L^{VA}_{\mu\nu} + a_\ell^2 L^{AA}_{\mu\nu}, \tag{B3}$$

where the neutral current is defined by $J^\mu = \bar\psi\gamma^\mu(v_\ell - a_\ell\gamma_5)\psi$ with

$$v_\ell = -1 + 4\sin^2\theta_W, \qquad a_\ell = -1 \qquad \text{for } \ell = e,\mu,\tau. \tag{B4}$$

In order to calculate the helicity representation of the lepton tensors in the helicity system one needs to evaluate

$$\widehat{L}^{(p)}_{mm'} = L^{(p)}_{\mu\nu}\varepsilon^\mu(m)\varepsilon^{*\,\nu}(m'), \qquad \widehat{L}^{(q)}_{nn'} = L^{(q)}_{\mu\nu}\varepsilon^\mu(n)\varepsilon^{*\,\nu}(n'). \tag{B5}$$

All objects referring to the helicity system are denoted by a hat symbol. The contractions are done in the helicity system using the representations (B1). Using the explicit forms (B1) one calculates

$$\begin{aligned} \widehat{L}^{VV(q)}_{\pm\pm} &= 2q^2, \quad \widehat{L}^{AA(q)}_{\pm\pm} = 2q^2(1-4\varepsilon), \quad \widehat{L}^{VA(q)}_{\pm\pm} = \widehat{L}^{AV(q)}_{\pm\pm} = \mp 2q^2(1-4\varepsilon)^{1/2}, \\ \widehat{L}^{VV(q)}_{00} &= 8q^2\varepsilon, \quad \widehat{L}^{AA(q)}_{00} = 0, \quad \widehat{L}^{VV(q)}_{tt} = 0, \\ \widehat{L}^{AA(q)}_{tt} &= 8q^2\varepsilon, \quad \widehat{L}^{VV,AA(q)}_{t0} = \widehat{L}^{VV,AA(q)}_{0t} = 0. \end{aligned} \tag{B6}$$

The ratio of helicity-flip and helicity-nonflip contributions can be seen to be given by $\hat{L}^{VV}_{00}/\hat{L}^{VV}_{\pm\pm} = 4\varepsilon$ and $\hat{L}^{AA}_{tt}/\hat{L}^{AA}_{\pm\pm} = 4\varepsilon/(1-4\varepsilon)$.

The components of the off-shell lepton tensor $L_{\lambda_Z\,\lambda'_Z}$ in the Higgs decay system (z axis along the Z^* direction) needed in the evaluation of Eq. (8) can be obtained by rotating the components of the lepton tensor $\widehat{L}_{\hat{\lambda}_Z\,\hat{\lambda}'_Z}$ defined in the helicity system according to (double indices are summed)

$$L_{\lambda_Z\,\lambda'_Z}(q^2,\cos\theta_q,\chi) = \sum_{J=0,1} d^J_{\lambda_Z\,\hat{\lambda}_Z}(\theta_q)\, d^J_{\lambda'_Z\,\hat{\lambda}'_Z}(\theta_q) e^{i(\lambda_Z-\lambda'_Z)\chi}\, \widehat{L}_{\hat{\lambda}_Z\,\hat{\lambda}'_Z}(q^2), \tag{B7}$$

where Wigner's d functions are given by

$$d^0(\theta) = 1, \qquad d^1_{mm'}(\theta) = \begin{pmatrix} \frac{1}{2}(1+\cos\theta) & -\frac{1}{\sqrt{2}}\sin\theta & \frac{1}{2}(1-\cos\theta) \\ \frac{1}{\sqrt{2}}\sin\theta & \cos\theta & -\frac{1}{\sqrt{2}}\sin\theta \\ \frac{1}{2}(1-\cos\theta) & \frac{1}{\sqrt{2}}\sin\theta & \frac{1}{2}(1+\cos\theta) \end{pmatrix}. \tag{B8}$$

The rows and columns in the spin-1 part of (B8) are labelled in the order $(+1,0,-1)$.

One obtains

$$\begin{aligned}
(2q^2)^{-1}L^{(q)}_{tt} &= 4\varepsilon a_\ell^2, \quad L^{(q)}_{t\pm} = L^{(q)}_{\pm t} = 0, \quad L^{(q)}_{t0} = L^{(q)}_{0t} = 0, \\
(2q^2)^{-1}L^{(q)}_{\pm\pm} &= \tfrac{1}{2}(1+\cos^2\theta)(v_\ell^2+a_\ell^2v_q^2) \pm 2v_\ell a_\ell v\cos\theta + 2\varepsilon v_\ell^2\sin^2\theta, \\
(2q^2)^{-1}L^{(q)}_{00} &= (v_\ell^2+a_\ell^2v_q^2)\sin^2\theta + 4\varepsilon v_\ell^2\cos^2\theta, \\
(2q^2)^{-1}L^{(q)}_{\pm 0} &= \tfrac{1}{2\sqrt{2}}\Big(\pm(v_\ell^2+a_\ell^2v_q^2)\sin 2\theta - 4v_\ell a_\ell v\sin\theta \mp 4\varepsilon v_\ell^2\sin 2\theta\Big)\, e^{\pm i\chi}, \\
L^{(q)}_{0\pm} &= L^{(q)\dagger}_{\pm 0}, \\
(2q^2)^{-1}L^{(q)}_{\pm\mp} &= \Big(\tfrac{1}{2}(v_\ell^2+a_\ell^2v_q^2)\sin^2\theta - 2\varepsilon v_\ell^2\sin^2\theta\Big)\, e^{\pm 2i\chi}.
\end{aligned} \tag{B9}$$

The corresponding expressions for the on-shell side lepton tensor $L_{p^2,\lambda_Z\,\lambda'_Z}(\cos\theta_p)$ can again be obtained by rotation. Note that in this case one has $\chi = 0$ as is evident from Fig. 1.

The spin-1 and spin-0 projections of the neutral lepton tensor needed in the main text are given by

$$\begin{aligned}
L_1(q^2) &= P_1^{\mu\nu}(q^2)L_{\mu\nu}(q^2) = L_{U+L}(q^2) = 4q^2\Big(v_\ell^2(1+2\varepsilon) + a_\ell^2(1-4\varepsilon)\Big), \\
L_0(q^2) &= P_0^{\mu\nu}(q^2)L_{\mu\nu}(q^2) = L_{tt}(q^2) = 4q^2a_\ell^2 2\varepsilon,
\end{aligned} \tag{B10}$$

where the spin-1 and spin-0 projectors read

$$P_1^{\mu\nu}(q^2) = -g^{\mu\nu} + \frac{q^\mu q^\nu}{q^2}, \qquad P_0^{\mu\nu}(q^2) = \frac{q^\mu q^\nu}{q^2}. \tag{B11}$$

Similar relations hold for the p side.

C Helicity representation of the charged-current lepton tensor

The lepton tensors are given by

$$\begin{aligned}
\text{on-shell side} \quad : \quad L_{\mu\nu}^{(p)} &= \mathrm{Tr}\left(\not{\ell}^- \gamma_\mu(1-\gamma_5)\not{\bar{\nu}}\gamma_\nu(1-\gamma_5)\right) \\
&= 8\left(\ell_\mu^- \bar{\nu}_\nu + \ell_\nu^- \bar{\nu}_\mu - \tfrac{1}{2}p^2 g_{\mu\nu} - i\epsilon_{\mu\nu\rho\sigma}p^\rho \ell^{-\sigma}\right), \\
\text{off-shell side} \quad : \quad L_{\mu\nu}^{(q)} &= \mathrm{Tr}\left((\not{\ell}^+ + m_\ell)\gamma_\mu(1-\gamma_5)\not{\nu}\gamma_\nu(1-\gamma_5)\right) \\
&= 8\left(\ell_\mu^+ \nu_\nu + \ell_\nu^+ \nu_\mu - \tfrac{1}{2}(q^2 - m_\ell^2)g_{\mu\nu} + i\epsilon_{\mu\nu\rho\sigma}q^\rho \ell^{+\sigma}\right).
\end{aligned} \tag{C1}$$

The kinematics for the off-shell q side is given by

$$\begin{aligned}
&q^\alpha = \sqrt{q^2}(1;0,0,0) \qquad \ell^{+\alpha} = \tfrac{1}{2}\sqrt{q^2}(1+\varepsilon;0,0,1-\varepsilon) \qquad \nu^\alpha = \tfrac{1}{2}\sqrt{q^2}(1-\varepsilon)(1;0,0,-1) \\
&\varepsilon^\mu(0) = (0;0,0,1) \qquad \varepsilon^\mu(\pm) = \frac{1}{\sqrt{2}}(0;\mp 1,-i,0) \qquad \varepsilon^\mu(t) = (1;0,0,0)
\end{aligned} \tag{C2}$$

(for the on-shell p side set $\varepsilon = 0$ and $q \to p$). The nonvanishing components of the helicity representations of the lepton tensors can then be evaluated to be

$$\begin{aligned}
\text{on-shell side} \quad &: \qquad \widehat{L}_{--}^{(p)} = 8m_W^2 \\
\text{off-shell side} \quad &: \quad \widehat{L}_{++}^{(q)} = 8q^2 v_\tau \qquad \widehat{L}_{00}^{(q)} = \widehat{L}_{0t}^{(q)} = \widehat{L}_{t0}^{(q)} = \widehat{L}_{tt}^{(q)} = 4m_\tau^2 v_\tau
\end{aligned} \tag{C3}$$

where $v_\tau = 1 - m_\tau^2/q^2 = 1 - \varepsilon$. Note that the ratio of helicity-flip and helicity-nonflip contributions are now given by e.g. $\widehat{L}_{00}^{(q)}/\widehat{L}_{++}^{(q)} = m_\tau^2/2q^2 = \varepsilon/2$.

As in the neutral-current case the components of the lepton tensor $L_{\lambda_W \lambda'_W}^{(q)}$ in the Higgs decay system (z axis along the W^{+*} direction) needed in the evaluation of Eq. (8) can be

obtained by rotating the components of the lepton tensor $\widehat{L}^{(q)}_{\hat{\lambda}_W\,\hat{\lambda}'_W}$ in the helicity system according to (double indices are summed)

$$L^{(q)}_{\lambda_W\,\lambda'_W}(\cos\theta_q,\chi) = \sum_{J,J'=0,1} d^J_{\lambda_W\,\hat{\lambda}_W}(\theta_q)\, d^{J'}_{\lambda'_W\,\hat{\lambda}'_W}(\theta_q) e^{i(\lambda_W-\lambda'_W)\chi}\, \widehat{L}^{(q)}_{\hat{\lambda}_W\,\hat{\lambda}'_W}. \tag{C4}$$

One obtains (the rows and columns of the matrix are ordered in the sequence $(t,+1,0,-1)$)

$$\begin{aligned}
&(2q^2v)^{-1} L_{\lambda_W\lambda'_W}(\cos\theta,\chi) \;=\\
&\begin{pmatrix}
0 & 0 & 0 & 0\\
0 & (1\mp\cos\theta)^2 & \mp\frac{2}{\sqrt{2}}(1\mp\cos\theta)\sin\theta e^{i\chi} & \sin^2\theta e^{2i\chi}\\
0 & \mp\frac{2}{\sqrt{2}}(1\mp\cos\theta)\sin\theta e^{-i\chi} & 2\sin^2\theta & \mp\frac{2}{\sqrt{2}}(1\pm\cos\theta)\sin\theta e^{i\chi}\\
0 & \sin^2\theta e^{-2i\chi} & \mp\frac{2}{\sqrt{2}}(1\pm\cos\theta)\sin\theta e^{-i\chi} & (1\pm\cos\theta)^2
\end{pmatrix}\\
&+\varepsilon\begin{pmatrix}
2 & -\frac{2}{\sqrt{2}}\sin\theta e^{i\chi} & 2\cos\theta & \frac{2}{\sqrt{2}}\sin\theta e^{i\chi}\\
-\frac{2}{\sqrt{2}}\sin\theta e^{-i\chi} & \sin^2\theta & -\frac{1}{\sqrt{2}}\sin 2\theta e^{i\chi} & -\sin^2\theta e^{2i\chi}\\
2\cos\theta & -\frac{1}{\sqrt{2}}\sin 2\theta e^{-i\chi} & 2\cos^2\theta & \frac{1}{\sqrt{2}}\sin 2\theta e^{i\chi}\\
\frac{2}{\sqrt{2}}\sin\theta e^{-i\chi} & -\sin^2\theta e^{-2i\chi} & \frac{1}{\sqrt{2}}\sin 2\theta e^{-i\chi} & \sin^2\theta
\end{pmatrix}
\end{aligned} \tag{C5}$$

The upper/lower signs refer to the decays $W^-\to\ell^-\bar{\nu}_\ell$ and $W^+\to\ell^+\nu_\ell$. The corresponding expressions for the on-shell-side lepton tensor $L^{(p)}_{\lambda_W\,\lambda'_W}(\cos\theta_p)$ can again be obtained by rotation. However, in this case one has $\chi=0$ as is evident from Fig. 7. Further, one has to use the lower signs in the matrices (C5).

The spin-1 and spin-0 projections of the charged lepton tensor are given by

$$\begin{aligned}
L^W_1(q^2) &= P^{\mu\nu}_1(q^2)L^{(q)}_{\mu\nu} = 8q^2(1-\varepsilon)\left(1+\tfrac{1}{2}\varepsilon\right),\\
L^W_0(q^2) &= P^{\mu\nu}_0(q^2)L^{(q)}_{\mu\nu} = 8q^2(1-\varepsilon)\tfrac{1}{2}\epsilon.
\end{aligned} \tag{C6}$$

References

[1] G. Aad *et al.* [ATLAS Collaboration], Phys. Lett. **B716** (2012) 1

[2] S. Chatrchyan *et al.* [CMS Collaboration], Phys. Lett. **B716** (2012) 30

[3] S. Chatrchyan *et al.* [CMS Collaboration], Phys. Rev. Lett. **110** (2013) 081803

[4] S. Chatrchyan *et al.* [CMS Collaboration], Phys. Rev. **D89** (2014) 092007

[5] G. Aad *et al.* [ATLAS Collaboration], Phys. Lett. **B726** (2013) 120

[6] G. Aad *et al.* [ATLAS Collaboration], arXiv:1503.03643 [hep-ex]

[7] S.Y. Choi, D.J. Miller, M.M. Mühlleitner and P.M. Zerwas, Phys. Lett. **B553** (2003) 61

[8] V.A. Kovalchuk, J. Exp. Theor. Phys. **107** (2008) 774

[9] Y. Gao, A.V. Gritsan, Z. Guo, K. Melnikov, M. Schulze and N.V. Tran, Phys. Rev. **D81** (2010) 075022

[10] A. De Rujula, J. Lykken, M. Pierini, C. Rogan and M. Spiropulu, Phys. Rev. **D82** (2010) 013003

[11] S. Bolognesi, Y. Gao, A.V. Gritsan, K. Melnikov, M. Schulze, N.V. Tran and A. Whitbeck, Phys. Rev. **D86** (2012) 095031

[12] P. Avery *et al.*, Phys. Rev. **D87** (2013) 055006

[13] Y. Sun, X.F. Wang and D.N. Gao, Int. J. Mod. Phys. **A29** (2014) 1450086

[14] G. Buchalla, O. Cata and G. D'Ambrosio, Eur. Phys. J. **C74** (2014) 2798

[15] M. Beneke, D. Boito and Y.M. Wang, JHEP **1411** (2014) 028

[16] J.S. Gainer, J. Lykken, K.T. Matchev, S. Mrenna and M. Park, Phys. Rev. **D91** (2015) 035011

[17] A. Menon, T. Modak, D. Sahoo, R. Sinha and H.Y. Cheng, Phys. Rev. **D89** (2014) 095021

[18] B. Bhattacherjee, T. Modak, S.K. Patra and R. Sinha, arXiv:1503.08924 [hep-ph]

[19] T.V. Zagoskin and A.Y. Korchin, arXiv:1504.07187 [hep-ph]

[20] J. Ellis, arXiv:1504.03654 [hep-ph]

[21] J. Ellis, M. K. Gaillard and D. V. Nanopoulos, arXiv:1504.07217 [hep-ph]

[22] A. Djouadi, arXiv:1505.01059 [hep-ph]

[23] A. Kadeer, J.G. Körner and U. Moosbrugger, Eur. Phys. J. **C59** (2009) 27

[24] J.G. Körner and G.A. Schuler, Phys. Lett. **B231** (1989) 306

[25] J.G. Körner and G.A. Schuler, Z. Phys. **C46** (1990) 93

[26] T. Gutsche, M.A. Ivanov, J.G. Körner, V.E. Lyubovitskij, P. Santorelli and N. Habyl, Phys. Rev. **D91** (2015) 074001

[27] B.A. Kniehl and O.L. Veretin, Phys. Rev. **D86** (2012) 053007

[28] M.E. Peskin and D.V. Schroeder, "An Introduction to quantum field theory," Reading, USA: Addison-Wesley (1995) 842 p

[29] J.G. Körner, arXiv:1402.2787 [hep-ph]

[30] L. Cappiello, O. Cata, G. D'Ambrosio and D.N. Gao, Eur. Phys. J. **C72** (2012) 1872 [Eur. Phys. J. **C72** (2012) 2208]

[31] S.R. Gevorkyan and M.H. Misheva, Eur. Phys. J. **C74** (2014) 2860

[32] J.G. Körner and G.A. Schuler, Z. Phys. **C38** (1988) 511 [Z. Phys. **C41** (1989) 690]

[33] M. Fischer, S. Groote, J.G. Körner and M.C. Mauser, Phys. Rev. **D67** (2003) 113008

[34] M. Fael, L. Mercolli and M. Passera, Phys. Rev. **D88** (2013) 093011

[35] S. Groote, J.G. Körner and L. Kaldamäe, "Identical particle and lepton mass effects in the decay $H \to \tau^+\tau^-\tau^+\tau^-$", in preparation

[36] S. Groote, J.G. Körner and P. Tuvike, Eur. Phys. J. **C72** (2012) 2177

[37] S. Groote, J.G. Körner and P. Tuvike, Eur. Phys. J. **C73** (2013) 2454

[38] G. Aad *et al.* [ATLAS and CMS Collaborations], Phys. Rev. Lett. **114** (2015) 191803

[39] K.A. Olive *et al.* [Particle Data Group Collaboration], Chin. Phys. **C38** (2014) 090001

[40] M. Gonzalez-Alonso and G. Isidori, Phys. Lett. **B733** (2014) 359

[41] W.Y. Keung and W.J. Marciano, Phys. Rev. **D30** (1984) 248

[42] A. Djouadi, Phys. Rept. **457** (2008) 1

[43] A. Denner, S. Heinemeyer, I. Puljak, D. Rebuzzi and M. Spira, Eur. Phys. J. **C71** (2011) 1753

[44] A. Grau, G. Panchieri and R.J.N. Phillips, Phys. Lett. **B251** (1990) 293

[45] Z. Zinonos, arXiv:1409.0343 [hep-ex]

[46] Y. Sakurai, arXiv:1409.2699 [hep-ex]

[47] D. Jeans, arXiv:1507.01700 [hep-ex]

[48] G. Aad *et al.* [ATLAS Collaboration], arXiv:1506.05623 [hep-ex]

[49] A. Bredenstein, A. Denner, S. Dittmaier and M.M. Weber, Phys. Rev. **D74** (2006) 013004

[50] A. Bredenstein, A. Denner, S. Dittmaier and M.M. Weber, JHEP **0702** (2007) 080